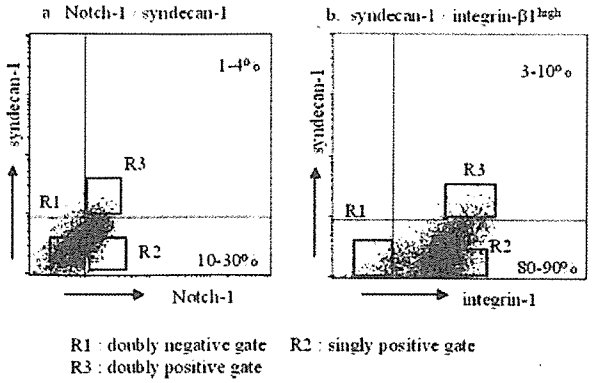

Fig. 3. **a,b:** Distribution and sorting gates (R1–R3) of the neurosphere cells in combined assays. Syndecan-1$^+$ cells mostly belonged to the integrin-β1$^+$ or Notch-1$^+$ cells. Three regions (R1, doubly negative; R2, singly positive; R3, doubly positive) as well as the control (all live cells) were sorted. The values are the ratios of singly positive or doubly positive cells to all live cells.

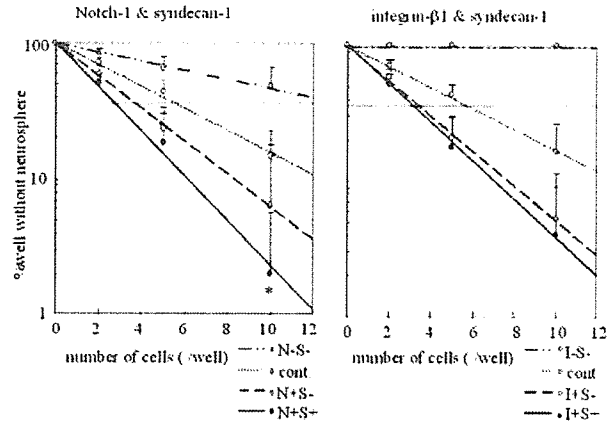

Fig. 4. Linear regression analysis of limiting dilution in combined assays. The neurosphere cells after 5–7 DIV were sorted by FACS using the combinated antigens and analyzed after culturing for 21 DIV. Each type of doubly positive cells formed significantly more neurospheres than the control cells. The N^+S^+ cells showed a significant difference from N^+S^- cells at 10 cells/well ($^*P < 0.05$). Solid line, doubly positive; dashed line, singly positive; dotted line, control; dashed and dotted line, double-negative population.

progeny. Among these surface markers, syndecan-1, Notch-1, integrin-β1, and Thy1.2 were found to be expressed in substantial amounts. The ratios of positive-to-total live cells for each antibody were 2–15%, 5–20%, 85–95%, 20–45%, respectively (Fig. 1). The other antigens were either not expressed or expressed at low and unreproducible levels on neurosphere cells.

Sorting of Cells Expressing Syndecan-1, Integrin-β1, and Notch-1 Increases the Frequency of NS-ICs

Statistical analysis of the NFR for singly positive and control populations for syndecan-1, integrin-β1, and Notch-1 revealed that the NFR for singly positive cells was significantly higher than that for control cells as well as that for negative cells at densities of 5, 10, and 20 cells/well (Fig. 2). The NFR of Thy 1.2^+ cells was also higher than that of the control cells at densities of 5–20 cells/well (data not shown). The EV was 3.4 for syndecan-1, 2.0 for integrin-$\beta1^{high}$, 1.9 for Notch-1, and 1.6 for Thy1.2, in decreasing order (Table I). Linear regression analysis revealed that one NS-IC was present among every 3.6 cells in the syndecan-1-positive population and among every 12.4 cells in the control population. That is, the syndecan-1-positive population was enriched with NS-ICs about 3.4 times compared with the control population. Syndecan-1 resulted in the best EV among all antigens tested (Table I). The NFRs for the three populations of cells with respect to integrin-β1, i.e., negative and positive with low-level and high-level expression, tended to be larger in this order (data not shown). Given these results, the following experiments focused on syndecan-1, integrin-β1, and Notch-1 expression.

Simultaneous staining of syndecan-1, integrin-β1, and Notch-1 revealed that most syndecan-1-positive cells (S^+) were included in the Notch-1-positive (N^+) or integrin-β1-positive (I^+) population, implying that the N^-S^+ or I^-S^+ populations rarely existed in N/S or S/I combinatory assays (Fig. 3a,b). Statistical analysis revealed that the NFR of the N^+S^+ population was significantly higher than that of the N^+S^- population at a density of 10 cells/well and moderately higher at densities of 2 and 5 cells/well ($P < 0.05$, n = 8–10 for every cell density; Fig. 4). However, the NFR of the S^+I^+ population was not significantly higher than that of the S^-I^+ population. EV was 2.1 for the N^+S^+ population and 1.9 for the S^+I^+population. This result means that, on average, every 2.6 cells in the N^+S^+ population contained one NS-IC, whereas every 5.4 cells in the control and every 3.6 cells in the N^+S^- population did (Table II). That is, the N^+S^+ population was 2.1-fold enriched with NS-ICs relative to the control population. Similarly, every 3.1 cells in the S^+I^+ population contained one NS-IC, whereas every 5.6 cells in the control and every 3.3 cells in the S^-I^+ population did. These results are summarized in Table II. EV was lower in the I/N assay (data not shown). These results suggest that the N^+S^+ fraction was the most efficient source of neurospheres.

In Vitro Multidifferentiation Potential of Cells Positive for Syndecan-1, Integrin-β1, and Notch-1

To demonstrate the pluripotency of the antigen-positive cells, we evaluated the differentiation capability of neurospheres derived from the sorted cells. We found that both primary and secondary neurospheres derived from cells positive for the syndecan-1, integrin-β1, and Notch-1 differentiated into the three neural lineages (Fig. 5). Furthermore, there was no preferential differentiation capacity toward the three neural lineages among cells expressing the three surface antigens (Fig. 6). These results suggest that the sorted positive populations have NS-IC-specific char-

TABLE II. NFV and EV in Combination Assays*

	N/S	S/I
NFV		
a	5.4	5.6
b	3.6	3.3
b′	2.6	3.1
EV		
a/b′	2.1	1.9

*The neurosphere cells after 5–7 DIV were sorted by FACS using the paired antigens and analyzed after culturing for 21DIV. NFV *a (for control), b (for single positive population), and b′ (for double positive population)* suggested that the N^+S^+ cells showed more efficient neurosphere formation than N^+S^- cells. EV *a/b′* shows that N/S was the best combination.

acteristics, including extensive proliferation and multidifferentiation.

Characterization of Primary Tissue Neural Cells and Determination of NFR

The usefulness of syndecan-1, Notch-1, and integrin-β1 for the isolation of NS-ICs from primary neural tissue was evaluated. These three antigens are also expressed on the surface of mouse primary striatum cells, at frequencies of 10–40%, 10–40%, and 40–70% of total live cells, respectively. Statistical analysis revealed that all three doubly positive populations of primary tissue cells more efficiently formed neurospheres than the control population at a density of 10 cells/well, in decreasing order of efficiency, N^+S^+, S^+I^+, and I^+N^+ ($P < 0.05$, n = 6–8 for every cell density; Fig. 7). Linear regression analysis with limiting dilution revealed that the NFV b′ of primary tissue cells for the N/S, S/I, and I/N combinations was 19.0, 23.5, and 52.9, respectively, while that for their control NFV a was 144 (Table III). On the other hand, the NFV b′ of the neurosphere cells after 5–7 DIV was 5.2, 5.1, and 5.5, respectively, in the same order, whereas that for control a was 9.5. The resulting EVs a/b′ of N/S, S/I, and I/N for primary tissue cells were 7.6, 6.1, and 2.7, respectively, whereas the EVs a/b′ for neurosphere cells after 5–7 DIV were 1.8, 1.9, and 1.7, respectively (Table III). These EVs for primary tissue cells were higher than those for neurosphere cells. For the N/S combination, the enrichment from primary tissue cells was 7.6 times greater than that from control cells, whereas the enrichment from neurosphere cells was 1.8 times greater than that from control cells. That is, the simultaneous expression of Notch-1 and syndecan-1 in primary tissue cells was more than four times more effective than such expression in neurosphere cells with respect to enhancing the isolation of NS-ICs.

SP and MP Cells Exhibit No Difference in NFR

It has been reported that SP cells in the bone marrow and in other organs have stem cell characteristics (Goodell et al., 1996; Jackson et al., 1999). To assess whether SP cells in neurosphere cells were enriched with NS-ICs, we assessed the NFRs of SP and MP cells in EGF-responsive neurospheres. SP cells constituted 1–5% of all live cells, whereas MP cells constituted ~70–80% (Fig. 8a). There was no significant difference in the NFRs between SP and MP cells ($P < 0.05$, n = 3–4 for every cell density; Fig. 8c), implying that SP characteristics do not lead to the enrichment of EGF-responsive NS-ICs.

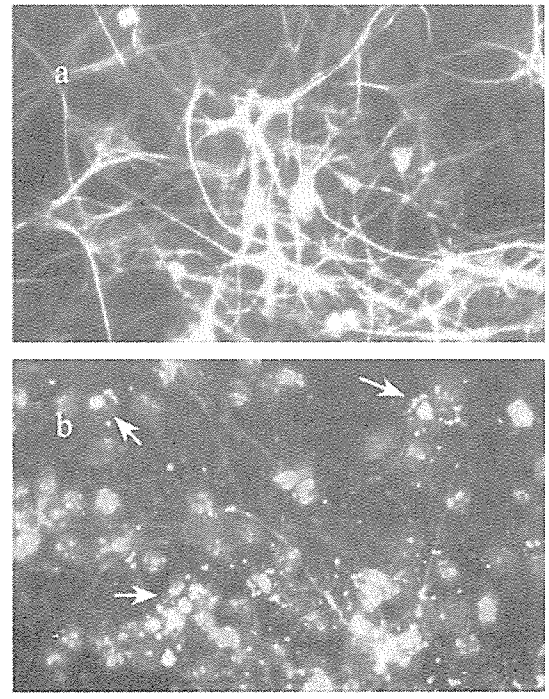

Fig. 5. Double immunocytochemistry of primary and secondary neurospheres in vitro. The primary and secondary neurospheres after culturing for 5–7 DIV were incubated in PLO-coated chamber slide containing 1% FCS/SFM for 4–6 DIV and were then demonstrated to differentiate into all three neural lineages. **a:** Green, GFAP; red, MAP2. **b:** Green, Galc; red, MAP2; blue, Hoechst 33342. Arrows, oligodendrocytes.

Multilineage Differentiation and Migration After Transplantation Into Neonatal Mouse Brain

For the purpose of verifying the in vivo potential of these sorted cells to migrate extensively into brain regions and differentiate into multilineage cell types, we transplanted sorted syndecan-1^+, integrin-$\beta1^+$, or Notch-1^+ cells derived from the brains of ~ E12.5–14.5 GFP embryos into the lateral ventricle of neonatal control mice. At 2–10 weeks after the transplantation, graft-derived GFP-positive cells were detected mainly around the region near the lateral and/or fourth ventricle, along with extensive regions of white matter, including the corpus callosum, internal capsule, fornix, fimbria, anterior commisure, and striatal white matter. Among these tissues, the corpus callosum was the most frequent site where the graft-derived GFP-positive cells were seen. Apart from this propensity toward white matter, the graft-derived cells were also observed in the hypothalamus, globus pallidus and caudoputamen, and inferior colliculus and cortex, and some cells were found in the rostral migratory pathway and olfactory bulb.

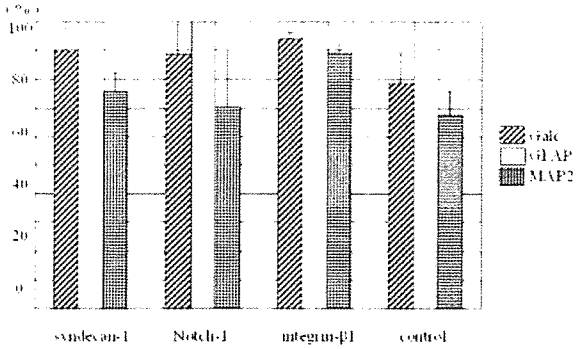

Fig. 6. Primary neurospheres after sorting with each surface antigen differentiated into all three neural lineages in vitro. About 50–100 primary neurospheres derived from the cells positive for each surface antigen were differentiated and doubly immunostained and were then examined for the three neural lineage markers by fluorescent microscopy. The vertical line shows the positive ratio (X/Y), which was determined from the number of neurospheres positive for each lineage-marker (X) divided by the number of all examined neurospheres (Y) for each. The neurospheres derived from the cells positive for each surface antigen differentiated into all three neural lineages in vitro, showing no preference for any of the three lineages.

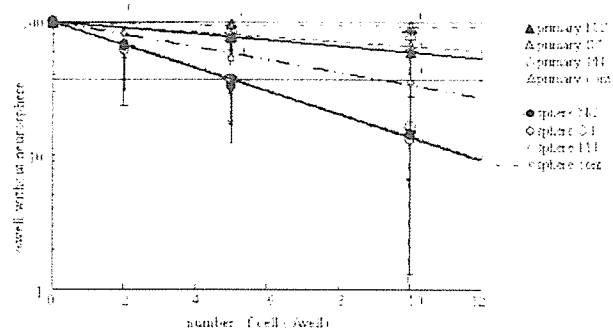

Fig. 7. Linear regression analysis with limiting dilution for the primary tissue cells and neurosphere cells after 5–7 DIV. The doubly positive cells from primary tissue cells also formed neurospheres more efficiently than control cells. (All three types of doubly positive cells at 10 cells/well, N^+S^+ and S^+I^+ at 5 cells/well, N^+S^+ only at 2 cells/well were significantly different from the control cells; at $^*P < 0.05$).

We found that graft-derived cells also differentiated into all three neural lineages (neurons, astrocytes, and oligodendrocytes). Double immunostaining with an anti-GFP antibody to detect the donor marker and antibodies specific for the three neural lineages revealed that these cells underwent multidifferentiation in vivo. The antibodies used recognized GFAP (Fig. 9a,b) and glutamine synthetase (Fig. 9c,d) as astroglia-specific markers, NeuN (Fig. 9e,f) and GABA (Fig. 9g,h) as neuron-specific markers, and NG2 (Fig. 9i,j) and MBP (Fig. 9k,l) as oligodendrocyte-specific markers. The transplanted cells extended many branched processes into the host tissue. Some of these cells, which resembled oligodendrocyte progenitors or which exhibited protoplasmic astrocyte morphology, seemed to surround the host neurons stained with the anti-NeuN antibody (Fig. 9B).

DISCUSSION

The neurosphere comprises a heterogeneous populations of cells, including cells characterized as NSCs, which can be demonstrated retrospectively by neurosphere reformation and differentiation into multiple lineages. Prospective methods for identifying NSCs and/or neural progenitors have been developed over the past several years (Uchida et al., 2000; Roy et al., 2000; Rietze et al., 2001; Kawaguchi et al., 2001). Analysis of NSC membrane properties, particularly compared with those of HSCs, have also been studied (Cai et al., 2003, 2004). Here we have demonstrated the usefulness of the syndecan-1, integrin-β1, and Notch-1 antigens expressed on both neurospheres and primary neural tissue cells for the enrichment of NS-ICs in vitro, by using a linear regression analysis with a limiting dilution assay employing FACS. We systematically examined the expression of cell surface markers characteristic of HSCs or progenitor cells as well as somatic stem cells and evaluated the NS-IC frequency of these populations. Although the three markers studied here were not specific for NSCs, their use allowed the prospective purification of NS-ICs. The neurosphere cells derived from cells sorted with these markers showed multidifferentiation potential, both in vitro and in vivo.

Syndecan-1, Integrin-β1, and Notch-1 Are Useful for Enriching NS-ICs

Syndecan-1^+, integrin-$\beta1^+$, Notch-1^+, and Thy1.2^+ cells each contained a higher proportion of NS-ICs than did control cells. Among these markers, Notch-1 is known to play a pivotal role in cell-fate decisions, especially with respect to "lateral inhibition," and is expressed in immature precursors of reciprocal adhesive cells (Irvin et al., 2001). Syndecan-1 is a transmembrane heparan sulfate proteoglycan that is considered to play roles important for growth factors, such as FGF-2 or transforming growth factor, leading to the modulation of signals from these cytokine receptors. Syndecan-1 is expressed abundantly in the neuroepithelial ventricular zone of the developing brain, where neural precursors proliferate (Ford-Perriss et al., 2003). The integrin-β1 chain is an intercellular adhesion molecule that forms heterodimers with several distinct α subunits in a broad variety of tissues. It is thought to be specific to dermal or neural precursor cells and to regulate their proliferation (Jacques et al., 1998). All of these molecules are thought to have some correlation with the characteristics of NSCs, but their contributions to "stemness" remain to be clarified.

EV measurements revealed that the singly positive cells for these three antigens formed neurospheres more efficiently (particularly, 3.4 times for syndecan-1) than did the control cells. Furthermore, in combinatory assays, the N^+S^+ population formed neurospheres more efficiently than the N^+S^- population. We conclude based on these results that the best procedure for the enrichment of NS-ICs from neurosphere cells is N^+S^+ selection. In our experiments, the NFR for N^+S^+ cells was about 38%, whereas that for N^-S^- cells was 7.6%. In a similar study, Capela et al. (2002) evaluated the

TABLE III. NFV and EV of Cells From Embryonic Brain and Neurospheres*

	N/S	I/S	I/N
Primary tissue cells			
NFV			
a	14.4	14.4	14.4
b′	19.0	23.5	52.9
EV			
a/b′	7.6	6.1	2.7
Neurosphere cells			
NFV			
a	9.5	9.5	9.5
b′	5.2	5.1	5.5
EV			
a/b′	1.8	1.9	1.7

*The embryonic brain tissue cells and neurosphere cells after 5–7 DIV were each divided into the three groups of doubly positive cells and controls, and sorted for analysis of NFV and EV after culturing for 21 DIV. NFV *a (for control population), b′ (for doubly positive population),* and EV *a/b′* revealed that the primary tissue cells formed neurospheres more efficiently than the neurosphere cells.

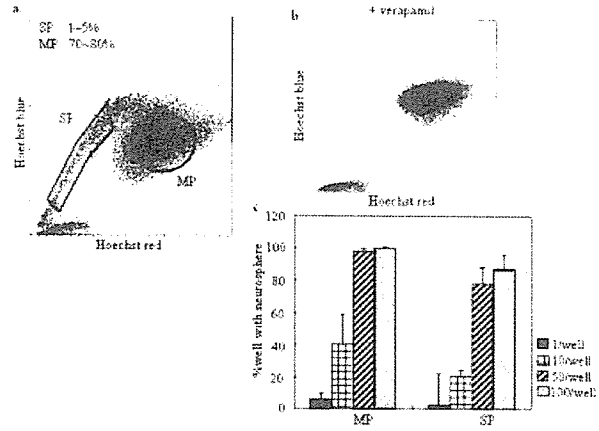

Fig. 8. Distribution (**a,b**) and NFR (**c**) for SP and MP in neurosphere cells. The neurosphere cells after culturing for 6 DIV were sorted according to SP or MP and analyzed after more culturing for 21 DIV. SP had almost dissapeared under the condition of additional verapamil (b). There was no significant difference in NFR between SP and MP cells (c).

NFR for cells expressing Lex/ssea1 on their surface. Their experiments showed that the NFR for Lex/ssea-1-positive cells was 22.1%, whereas that for Lex/ssea-1-negative cells was less than 1% in the adult SVZ. The NFR for the N^+S^+ population in our study was high, although a direct comparison between the two studies could not be made, because we used neurosphere cells derived from embryonic SVZ cells whereas Capela et al. used cells derived from adult SVZ cells. Both studies demonstrated that the use of combinatory N/S antigens is a potent method for NS-IC selection. Interestingly, Rietze et al. (2001) demonstrated that larger cells formed neurospheres more efficiently than smaller ones, as shown by neurosphere formation analysis after sorting of primary tissue cells according to the size difference. Their NS-IC frequency was 1 of 149 cells, which was more than 12 μm, and 1 of 1.28 cells, which was more than 12 μm and with low-level expression of both peanut agglutinin and heat-stable antigen. Their results were much better than ours when using N^+S^+ selection, and in addition they used primary tissue cells, which show lower NS-IC frequency than neurosphere cells. We also found preliminarily that there tended to be little difference in NFR between triply positive cells for surface antigens ($S^+I^+N^+$) and the N^+S^+ cells (data not shown). This might be because the positive populations of each surface antigen were overlapping, at least partially. In our assay, the syndecan-1-, integrin-β1-, or Notch-1-positive cells tended to be larger than cells negative for each of these markers and to be greater when their fluorescence intensity was stronger (data not shown). These results suggest that cell size should also be useful for isolating NSCs.

Syndecan-1^+, Integrin-β1^+, and Notch-1^+ Cells in Primary Neural Tissues Also Efficiently Form Neurospheres

Syndecan-1, integrin-β1, and Notch-1 were also useful for characterizing NSCs from primary neural tissues as well as from neurospheres. Two characteristic points were noted concerning the enrichment from primary tissue cells compared with that from neurosphere cells. First, the EV from primary tissue cells was higher than that from neurosphere cells; in particular, it was about four times higher in the N^+S^+ population (Table III). Second, the EVs for primary tissue cells varied more markedly depending on the combinations of these three antigens than the EVs for neurosphere cells. EV in the case of I/N was 2.7, but that for N/S or I/S was 7.6 or 6.1. Differences of the contributory degrees of these markers were suspected between primary tissue cells and neurospheres for characterizing NS-ICs. Taken together, these results suggest that syndecan-1 is also the most useful marker for characterizing NS-ICs from primary neural tissues.

Sorted Cells With Syndecan-1, Integrin-β1, or Notch-1 Expression Differentiate Into Three Lineages Both In Vitro and In Vivo

We confirmed that syndecan-1^+, integrin-β1^+, and Notch-1^+ cells differentiate into all three neural lineages in vitro. Mitome et al. (2001) and Winkler et al. (1998) concluded that EGF-responsive neurosphere cells appear to differentiate predominantly into glial cells in vivo, in contrast to their in vitro multidifferentiality. Our result was basically in agreement with their observations; on the other hand, neuronal differentiation could also be detected easily all over the field in vivo after transplantation. Therefore, it was suspected that cells with these markers in neurospheres had greater differentiational potential than just the cells in neurospheres used by Mitome et al. and Wincler et al., implying the feasibility of these antigens for isolating NSCs prospectively. However, differentiation into the glial lineage was still dominant in vivo, suggesting that factors other than the intrinsic ones within NSCs, such as

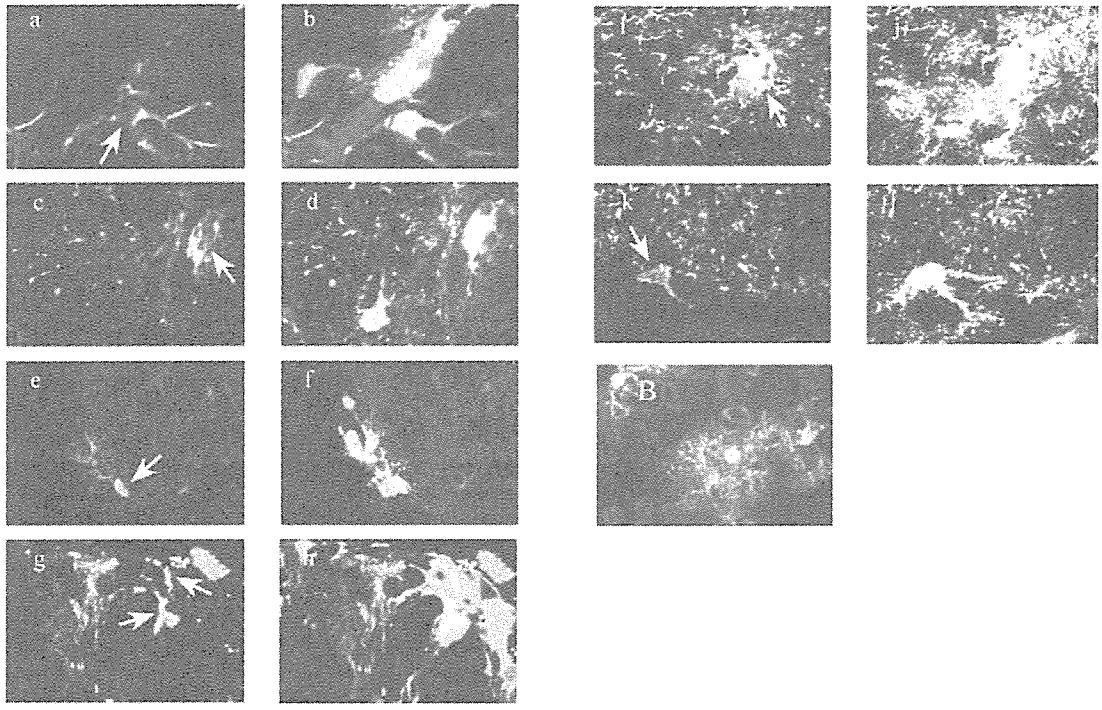

Fig. 9. Double-immunostaining of transplanted GFP cells (green; anti-GFP antibody) revealed the multidifferentiational potentiality in vivo of cells sorted according to the surface antigens. **a–l:** The two images in the same row are in the same visual field. Red in a and b, GFAP; c and d, glutamine synthetase; e and f, NeuN; g and h, GABA; i and j, NG2; k and l, MBP. **B:** The transplanted GFP cell extended among the host cells with numerous, branched processes (red, NeuN).

microenvironmental factors, might contribute to the cell-lineage decision during differentiation.

In a report supporting this notion, neurosphere cells derived from the ganglionic eminence were revealed to express neuronal phenotypes depending on their environment and not on their region of origin (Olsson et al., 1997; Hitoshi et al., 2002). On the other hand, it was reported that donor-specific factors, including the in vitro conditions for cell expansion, affected the fate of transplanted cells in vivo. In vitro priming of neurospheres with specific cytokines during expansion led them to differentiate predominantly into the neuronal lineage (Wu et al., 2002). As previously mentioned, donor cells derived from EGF-responsive progenitors might have a propensity for glial differentiation after transplantation (Winkler et al., 1998) but the donor cells from EGF-, FGF-, and leukemia inhibitory factor (LIF)-responsive progenitors were demonstrated to have a stronger propensity for neuronal differentiation (Fricker et al., 1999). Although neuronal differentiation was confirmed in our experiments, the number of neuronal cells was still small. The in vitro priming procedure should be examined regarding its ability to cause predominant differentiation into neuronal lineages in vivo, when applied along with the FACS method.

NFRs of SP and MP Cells Are Not Significantly Different

Hulspas and Quesenberry (2000) reported that SP cells derived from the murine embryonic brain were not significantly enriched for NS-ICs, as determined in single-cell culture assays. Moreover, according to Rietze et al.'s results, cells that exhibit excellent neurosphere-forming activity were brightly labeled with the dye Hoechst 33342. Also in our study, the NFRs of SP and MP cells were not significantly different. These results suggest that SP characteristic could not be a marker for the isolation of stem cells in the neural system. Our studies also suggested that each of the populations positive for syndecan-1, integrin-β1, and Notch-1 tended to be distributed in a rather brighter position in FACS analysis, i.e., in MP but not in SP, than the negative populations. SP as well as MP cells did not seem to show characteristic distribution according to the three antibodies (data not shown).

However, recently Kim and Morshead (2003) reported that SP cells were enriched in the EGF- and FGF-responsive stem cells, which seems to contradict our results. We also observed the superiority of NFR for EGF- and FGF-responsive NS-ICs compared with EGF-responsive NS-ICs in assays using spinal cord cells (data not shown).

We believe it likely that the difference in mitogens used in the assays can partially account for the differences between their results and ours. These speculation might be supported by Maruyama et al.'s (2002) report that NS-ICs in SP cells were not uniform and varied with regard to development as indicated by their cell size or surface antigen.

Here we have demonstrated that syndecan-1$^+$, integrin-β1$^+$, and Notch-1$^+$ cells form neurospheres efficiently and that these cells can differentiate into the three neural lineages in vitro and in vivo. These markers are useful for the isolation of NS-ICs prospectively, which will lead to further investigation of NSCs.

REFERENCES

Akashi K, Traver D, Miyamoto T, Weissman IL. 2000. A clonogenic common myeloid progenitor that gives rise to all myeloid lineages. Nature 404:193–197.

Bjornson CR, Rietze RL, Reynolds BA, Magli MC, Vescovi AL. 1999. Turning brain into blood: a hematopoietic fate adopted by adult neural stem cells in vivo. Science 283:534–537.

Cai J, Limke TL, Ginis I, Rao MS. 2003. Identifying and tracking neural stem cells. Blood Cells Mol Dis 31:18–27.

Cai J, Cheng A, Luo Y, Lu C, Mattson MP, Rao MS, Furukawa K. 2004. Membrane properties of rat embryonic multipotent neural stem cells. J Neurochem 88:212–226.

Capela A, Temple S. 2002. LeX/ssea-1 is expressed by adult mouse CNS stem cells, identifying them as nonependymal. Neuron 35:865–875.

Doetsch F, Garcia-Verdugo JM, Alvarez-Buylla A. 1997. Cellular composition and three-dimensional organization of the subventricular germinal zone in the adult mammalian brain. J Neurosci 17:5046–5061.

Engstrom CM, Demers D, Dooner M, McAuliffe C, Benoit BO, Stencel K, Joly M, Hulspas R, Reilly JL, Savarese T, Recht LD, Ross AH, Quesenberry PJ. 2002. A method for clonal analysis of epidermal growth factor-responsive neural progenitors. J Neurosci Methods 117:111–121.

Ford-Perriss M, Turner K, Guimond S, Apedaile A, Haubeck HD, Turnbull J, Murphy M. 2003. Localisation of specific heparan sulfate proteoglycans during the proliferative phase of brain development. Dev Dyn 227:170–184.

Fricker RA, Carpenter MK, Winkler C, Greco C, Gates MA, Bjorklund A. 1999. Site-specific migration and neuronal differentiation of human neural progenitor cells after transplantation in the adult rat brain. J Neurosci 19:5990–6005.

Gage FH, Coates PW, Palmer TD, Kuhn HG, Fisher LJ, Suhonen JO, Peterson DA, Suhr ST, Ray J. 1995. Survival and differentiation of adult neuronal progenitor cells transplanted to the adult brain. Proc Natl Acad Sci U S A 92:11879–11883.

Goodell MA, Brose K, Paradis G, Conner AS, Mulligan RC. 1996. Isolation and functional properties of murine hematopoietic stem cells that are replicating in vivo. J Exp Med 183:1797–1806.

Gritti A, Parati EA, Cova L, Frolichsthal P, Galli R, Wanke E, Faravelli L, Morassutti DJ, Roisen F, Nickel DD, Vescovi AL. 1996. Multipotential stem cells from the adult mouse brain proliferate and self-renew in response to basic fibroblast growth factor. J Neurosci 16:1091–1100.

Hitoshi S, Tropepe V, Ekker M, van der Kooy D. 2002. Neural stem cell lineages are regionally specified, but not committed, within distinct compartments of the developing brain. Development 129:233–244.

Hockfield S, McKay RD. 1985. Identification of major cell classes in the developing mammalian nervous system. J Neurosci 5:3310–3328.

Hulspas R, Quesenberry PJ. 2000. Characterization of neurosphere cell phenotypes by flow cytometry. Cytometry 40:245–250.

Irvin DK, Zurcher SD, Nguyen T, Weinmaster G, Kornblum HI. 2001. Expression patterns of Notch1, Notch2, and Notch3 suggest multiple functional roles for the Notch-DSL signaling system during brain development. J Comp Neurol 436:167–181.

Jackson KA, Mi T, Goodell MA. 1999. Hematopoietic potential of stem cells isolated from murine skeletal muscle. Proc Natl Acad Sci U S A 96:14482–14486.

Jacques TS, Relvas JB, Nishimura S, Pytela R, Edwards GM, Streuli CH, ffrench-Constant C. 1998. Neural precursor cell chain migration and division are regulated through different beta1 integrins. Development 125:3167–3177.

Johansson CB, Momma S, Clarke DL, Risling M, Lendahl U, Frisen J. 1999. Identification of a neural stem cell in the adult mammalian central nervous system. Cell 96:25–34.

Kaneko Y, Sakakibara S, Imai T, Suzuki A, Nakamura Y, Sawamoto K, Ogawa Y, Toyama Y, Miyata T, Okano H. 2000. Musashi1: an evolutionally conserved marker for CNS progenitor cells including neural stem cells. Dev Neurosci 22:139–153.

Kanemura Y, Mori H, Kobayashi S, Islam O, Kodama E, Yamamoto A, Nakanishi Y, Arita N, Yamasaki M, Okano H, Hara M, Miyake J. 2002. Evaluation of in vitro proliferative activity of human fetal neural stem/progenitor cells using indirect measurements of viable cells based on cellular metabolic activity. J Neurosci Res 69:869–879.

Kawaguchi A, Miyata T, Sawamoto K, Takashita N, Murayama A, Akamatsu W, Ogawa M, Okabe M, Tano Y, Goldman SA, Okano H. 2001. Nestin-EGFP transgenic mice: visualization of the self-renewal and multipotency of CNS stem cells. Mol Cell Neurosci 17:259–273.

Kim M, Morshead CM. 2003. Distinct populations of forebrain neural stem and progenitor cells can be isolated using side-population analysis. J Neurosci 23:10703–10709.

Kuhn HG, Dickinson-Anson H, Gage FH. 1996. Neurogenesis in the dentate gyrus of the adult rat: age-related decrease of neuronal progenitor proliferation. J Neurosci 16:2027–2033.

Kuhn HG, Winkler J, Kempermann G, Thal LJ, Gage FH. 1997. Epidermal growth factor and fibroblast growth factor-2 have different effects on neural progenitors in the adult rat brain. J Neurosci 17:5820–5829.

Lendahl U, Zimmerman LB, McKay RD. 1990. CNS stem cells express a new class of intermediate filament protein. Cell 60:585–595.

Levison SW, Goldman JE. 1993. Both oligodendrocytes and astrocytes develop from progenitors in the subventricular zone of postnatal rat forebrain. Neuron 10:201–212.

Lois C, Alvarez-Buylla A. 1993. Proliferating subventricular zone cells in the adult mammalian forebrain can differentiate into neurons and glia. Proc Natl Acad Sci U S A 90:2074–2077.

Luskin MB. 1993. Restricted proliferation and migration of postnatally generated neurons derived from the forebrain subventricular zone. Neuron 11:173–189.

Mitome M, Low HP, van den Pol A, Nunnari JJ, Wolf MK, Billings-Gagliardi S, Schwartz WJ. 2001. Towards the reconstruction of central nervous system white matter using neural precursor cells. Brain 124:2147–2161.

Morrison SJ, Weissman IL. 1994. The long-term repopulating subset of hematopoietic stem cells is deterministic and isolatable by phenotype. Immunity 1:661–673.

Morshead CM, Reynolds BA, Craig CG, McBurney MW, Staines WA, Morassutti D, Weiss S, van der Kooy D. 1994. Neural stem cells in the adult mammalian forebrain: a relatively quiescent subpopulation of subependymal cells. Neuron 13:1071–1082.

Murayama A, Matsuzaki Y, Kawaguchi A, Shimazaki T, Okano H. 2002. Flow cytometric analysis of neural stem cells in the developing and adult mouse brain. J Neurosci Res 69:837–847.

Okabe M, Ikawa M, Kominami K, Nakanishi T, Nishimune Y. 1997. "Green mice" as a source of ubiquitous green cells. FEBS Lett 407:313–319.

Okano H. 2002a. Neural stem cells: progression of basic research and perspective for clinical application. Keio J Med 51:115–128.

Okano H. 2002b. Stem cell biology of the central nervous system. J Neurosci Res 69:698–707.

Olsson M, Bentlage C, Wictorin K, Campbell K, Bjorklund A. 1997. Extensive migration and target innervation by striatal precursors after grafting into the neonatal striatum. Neuroscience 79:57–78.

Osawa M, Hanada K, Hamada H, Nakauchi H. 1996. Long-term lymphohematopoietic reconstitution by a single CD34-low/negative hematopoietic stem cell. Science 273:242–245.

Palmer TD, Ray J, Gage FH. 1995. FGF-2-responsive neuronal progenitors reside in proliferative and quiescent regions of the adult rodent brain. Mol Cell Neurosci 6:474–486.

Pevny LH, Sockanathan S, Placzek M, Lovell-Badge R. 1998. A role for SOX1 in neural determination. Development 125:1967–1978.

Ramalho-Santos M, Yoon S, Matsuzaki Y, Mulligan RC, Melton DA. 2002. "Stemness": transcriptional profiling of embryonic and adult stem cells. Science 298:597–600.

Reynolds BA, Weiss S. 1992. Generation of neurons and astrocytes from isolated cells of the adult mammalian central nervous system. Science 255:1707–1710.

Reynolds BA, Weiss S. 1996. Clonal and population analyses demonstrate that an EGF-responsive mammalian embryonic CNS precursor is a stem cell. Dev Biol 175:1–13.

Richards LJ, Kilpatrick TJ, Bartlett PF. 1992. De novo generation of neuronal cells from the adult mouse brain. Proc Natl Acad Sci U S A 89:8591–8595.

Rietze RL, Valcanis H, Brooker GF, Thomas T, Voss AK, Bartlett PF. 2001. Purification of a pluripotent neural stem cell from the adult mouse brain. Nature 412:736–739.

Roy NS, Wang S, Jiang L, Kang J, Benraiss A, Harrison-Restelli C, Fraser RA, Couldwell WT, Kawaguchi A, Okano H, Nedergaard M, Goldman SA. 2000. In vitro neurogenesis by progenitor cells isolated from the adult human hippocampus. Nat Med 6:271–277.

Sakakibara S, Okano H. 1997. Expression of neural RNA-binding proteins in the postnatal CNS: implications of their roles in neuronal and glial cell development. J Neurosci 17:8300–8312.

Sakakibara S, Imai T, Hamaguchi K, Okabe M, Aruga J, Nakajima K, Yasutomi D, Nagata T, Kurihara Y, Uesugi S, Miyata T, Ogawa M, Mikoshiba K, Okano H. 1996. Mouse-Musashi-1, a neural RNA-binding protein highly enriched in the mammalian CNS stem cell. Dev Biol 176:230–242.

Salner AL, Obbagy JE, Hellman S. 1982. Differing stem cell self-renewal of lectin-separated murine bone marrow fractions. JNCI 68:639–641.

Svendsen CN, ter Borg MG, Armstrong RJ, Rosser AE, Chandran S, Ostenfeld T, Caldwell MA. 1998. A new method for the rapid and long term growth of human neural precursor cells. J Neurosci Methods 85:141–152.

Terskikh AV, Easterday MC, Li L, Hood L, Kornblum HI, Geschwind DH, Weissman IL. 2001. From hematopoiesis to neuropoiesis: evidence of overlapping genetic programs. Proc Natl Acad Sci U S A 98:7934–7939.

Tropepe V, Sibilia M, Ciruna BG, Rossant J, Wagner EF, van der Kooy D. 1999. Distinct neural stem cells proliferate in response to EGF and FGF in the developing mouse telencephalon. Dev Biol 208:166–188.

Uchida N, Weissman IL. 1992. Searching for hematopoietic stem cells: evidence that Thy-1.1lo Lin^- $Sca\text{-}1^+$ cells are the only stem cells in C57BL/Ka-Thy-1.1 bone marrow. J Exp Med 175:175–184.

Uchida N, Jerabek L, Weissman IL. 1996. Searching for hematopoietic stem cells. II. The heterogeneity of Thy-1.1(lo)Lin(−/lo)$Sca\text{-}1^+$ mouse hematopoietic stem cells separated by counterflow centrifugal elutriation. Exp Hematol 24:649–659.

Uchida N, Buck DW, He D, Reitsma MJ, Masek M, Phan TV, Tsukamoto AS, Gage FH, Weissman IL. 2000. Direct isolation of human central nervous system stem cells. Proc Natl Acad Sci U S A 97:14720–14725.

Vescovi AL, Reynolds BA, Fraser DD, Weiss S. 1993. bFGF regulates the proliferative fate of unipotent (neuronal) and bipotent (neuronal/astroglial) EGF-generated CNS progenitor cells. Neuron 11:951–966.

Winkler C, Fricker RA, Gates MA, Olsson M, Hammang JP, Carpenter MK, Bjorklund A. 1998. Incorporation and glial differentiation of mouse EGF-responsive neural progenitor cells after transplantation into the embryonic rat brain. Mol Cell Neurosci 11:99–116.

Wu P, Tarasenko YI, Gu Y, Huang LY, Coggeshall RE, Yu Y. 2002. Region-specific generation of cholinergic neurons from fetal human neural stem cells grafted in adult rat. Nat Neurosci 5:1271–1278.

THE JOURNAL OF BIOLOGICAL CHEMISTRY
Vol. 280, No. 20, Issue of May 20, pp. 19682–19688, 2005
Printed in U.S.A.

Acetylation of GATA-4 Is Involved in the Differentiation of Embryonic Stem Cells into Cardiac Myocytes*[S]

Received for publication, November 3, 2004, and in revised form, February 9, 2005
Published, JBC Papers in Press, March 13, 2005, DOI 10.1074/jbc.M412428200

Teruhisa Kawamura‡, Koh Ono‡, Tatsuya Morimoto§, Hiromichi Wada§, Maretoshi Hirai§, Kyoko Hidaka¶, Takayuki Morisaki¶, Toshio Heike‖, Tatsutoshi Nakahata‖, Toru Kita§, and Koji Hasegawa‡

From the ‡Division of Translational Research, Kyoto Medical Center, National Hospital Organization, 1-1 Mukaihata-cho, Fukakusa, Fushimi-ku, Kyoto 612-8555, the Departments of §Cardiovascular Medicine and ‖Pediatrics, Graduate School of Medicine, Kyoto University, 54 Kawara-cho, Shogoin, Sakyo-ku, Kyoto 606-8507, and the ¶Department of Bioscience, National Cardiovascular Center Research Institute, 5-7-1 Fujishirodai, Suita, Osaka 565-8565, Japan

Differentiation of embryonic stem (ES) cells into cardiac myocytes requires activation of a cardiac-specific gene program. Histone acetyltransferases (HATs) and histone deacetylases (HDACs) govern gene expression patterns by being recruited to target genes through association with specific transcription factors. One of the HATs, p300, serves as a coactivator of cardiac-specific transcription factors such as GATA-4. The HAT activity of p300 is required for acetylation and DNA binding of GATA-4 and its full transcriptional activity as well as for promotion of a transcriptionally active chromatin configuration. However, the roles of HATs and HDACs in post-translational modification of GATA-4 during the differentiation of ES cells into cardiac myocytes remain unknown. In an ES cell model of developing embryoid bodies, an acetylated form of GATA-4 and its DNA binding increased concomitantly with the expression of p300 during the differentiation of ES cells into cardiac myocytes. Treatment of ES cells with trichostatin A (TSA), a specific HDAC inhibitor, induced acetylation of histone-3/4 near GATA sites within the atrial natriuretic factor promoter. In addition, TSA augmented the increase in an acetylated form of GATA-4 and its DNA binding during the ES cell differentiation. Finally, TSA facilitated the expression of green fluorescence protein under the control of the cardiac-specific Nkx-2.5 promoter and of endogenous cardiac β-myosin heavy chain during the differentiation. These findings demonstrate that acetylation of GATA-4 as well as of histones is involved in the differentiation of ES cells into cardiac myocytes.

During embryogenesis, cell type-specific gene expression plays a pivotal role in the determination of cell fate determination, including differentiation, proliferation, and apoptosis. In contrast to other cell types, cardiac muscle cells are highly organized and their developmental processes require a number of cell type-specific transcription factors (1). Among these, a zinc finger protein, GATA-4, is expressed at the earliest stage during heart development. In addition, embryonic stem (ES)[1] cell lines overexpressing GATA-4 show enhancement of cardiac myocyte differentiation, whereas GATA-4-deficient ES cell lines are impaired in differentiation. These findings suggest that GATA-4 is one of the DNA binding transcription factors regulating cardiac muscle cell differentiation (2).

Histone acetyltransferases (HATs) and histone deacetylases (HDACs) regulate gene expression patterns by affecting chromatin structure. These regulators are recruited to target genes in association with specific DNA binding transcription factors. HATs facilitate chromatin opening by acetylating the N-terminal tails of nucleosomal histones, which are rich in lysine residues, thus promoting active transcription (3). Conversely, HDACs deacetylate lysine residues and induce compaction of chromatin, making the access of transcription factors to nearby promoters more difficult and thereby resulting in gene silencing (4). A transcriptional coactivator, p300, serves as one of the intrinsic HATs and plays central roles in a wide range of cellular processes, including proliferation, apoptosis, and differentiation (3, 5). In addition, p300 is able to acetylate several DNA binding transcription factors and enhance their DNA binding activities (3). For example, p300 acetylates p53, increases its DNA binding activity, and activates the transcription of p53-inducible genes, contributing to cell cycle arrest or apoptosis (6, 7). In cardiac myocytes, p300 acetylates GATA-4, enhances its DNA binding, and plays an important role in the transactivation of hypertrophy-responsive genes (8). However, the roles of HATs and HDACs in post-translational modification of GATA-4 during the differentiation of ES cells into cardiac myocytes remain unknown. Specifically, we would like to know whether the acetylation of GATA-4 occurs in ES cells during their differentiation into cardiac myocytes and, if so, whether pharmacological augmentation of the acetylation could facilitate the differentiation. The present study was performed to address these questions.

MATERIALS AND METHODS

Cell Line and Cell Culture of Embryonic Stem Cells—The 129/Ola-derived ES cell lines we used in the present study were ht7 and its derivative (Nkx2.5-GFP ES cells) in which green fluorescent protein (GFP) is knocked into the Nkx2.5 locus (9). These cells were maintained and differentiated as previously described (9). In brief, the cells were grown on gelatinized dishes without feeder cells by using culture me-

* This work was supported in part by the Advanced and Innovational Research Program in Life Science and grants from the Ministry of Education, Science, and Culture of Japan (to T. Kita and K. Hasegawa). The costs of publication of this article were defrayed in part by the payment of page charges. This article must therefore be hereby marked "*advertisement*" in accordance with 18 U.S.C. Section 1734 solely to indicate this fact.

[S] The on-line version of this article (available at http://www.jbc.org) contains a supplemental figure.

** To whom correspondence should be addressed. Tel.: 81-75-641-9161; Fax: 81-75-641-9252; E-mail: koj@kuhp.kyoto-u.ac.jp.

[1] The abbreviations used are: ES, embryonic stem; HAT, histone acetyltransferase; HDAC, histone deacetylase; TSA, trichostatin A; GFP, green fluorescent protein; EB, embryoid body; EMSA, electrophoretic mobility shift assay; ANF, atrial natriuretic factor; MHC, myosin heavy chain; GAPDH, glyceraldehyde-3-phosphate dehydrogenase; WT, wild type.

dium containing Glasgow-modified Eagle's medium, 1000 units/ml leukemia inhibitory factor (Chemicon International), 100 mg/ml hygromycin (Invitrogen), 10% heat-inactivated fetal calf serum, 1 × nonessential amino acids, 1 mmol/liter sodium pyruvate, 50 units/ml penicillin, 0.05 mg/ml streptomycin, and 0.1 mmol/liter 2-mercaptoethanol. Differentiation of ES cells was induced through formation of embryoid bodies (EBs). After incubation in hanging drops for 2 days, 60 EBs were transferred into 10-cm bacterial Petri dishes together with 10 ml of differentiation medium and cultured as floating EBs until dissociation for the experiments.

Western Blotting, Immunoprecipitation, and Analysis of the Acetylation State of GATA-4—Nuclear protein extracts from ES cells were prepared as previously described (8). Immunoprecipitation and Western blotting for p300, GATA-4, and β-actin were performed as previously described (8). Briefly, aliquots of the lysates containing 100 μg of protein were immunoprecipitated by incubating with goat anti-GATA-4 polyclonal antibody (Santa Cruz Biotechnology) or normal goat IgG in low stringency buffer for 16 h at 4 °C and then incubating with protein G beads (Amersham Biosciences) for 2 h at 4 °C. The precipitate was washed four times in the same buffer and subjected to Western blotting by using rabbit polyclonal antibody against acetylated lysine (Cell Signaling) or rabbit anti-GATA-4 polyclonal antibody (Santa Cruz Biotechnology). The detection of acetylated GATA-4 was also analyzed by pulse labeling as previously described (8). Briefly, EBs were resuspended in 2.5 ml of medium containing 0.05 mCi of [1-^{14}C]acetic acid sodium salt/ml (200 μCi/ml; Amersham Biosciences) and incubated for 3 h. Ethanol, the solvent of [1-^{14}C]acetic acid sodium salt, was removed by evaporation to minimize the cytotoxic effect of the ethanol in the culture medium. Nuclear extracts from these cells were immunoprecipitated using goat anti-GATA-4 antibody (Santa Cruz Biotechnology) or normal goat IgG in low stringency buffer for 16 h at 4 °C and incubated with protein G beads for 1 h at 4 °C. The precipitate was washed four times in the same buffer, resuspended in 50 μl of sodium dodecyl sulfate (SDS) lysis buffer, heated to 95 °C for 2 min, electrophoresed in an SDS-polyacrylamide gel, fixed, and autoradiographed using a bioimaging analyzer (BAS 2000; FUJIX).

Electrophoretic Mobility Shift Assays (EMSAs)—EMSAs were carried out as previously described (8). The sequence of the sense strands of the double-stranded oligonucleotides containing a GATA-4 site in the endothelin-1 promoter were as follows: Wt-GATA, 5′-CCTCTAGAGCCGGGTCT TATCTCCGGCTGCACGTTGC-3′, and Mut-GATA, 5′-CCTCTAGAGCCGGGTCTGCACTCCGGCTGCACGTTGC-3′ (mutated sequence is underlined). We also used a double-stranded oligonucleotide that contained the Sp-1 binding site as a control probe (purchased from Santa Cruz Biotechnology, Inc.).

Acid Extraction of Proteins from ES Cells and Detection of Histone Acetylation—Histones were isolated by acid extraction using a commercial kit (Upstate) according to the manufacturer's recommendations. In brief, cells were washed with phosphate-buffered saline, resuspended in lysis buffer with 0.2 mol/liter hydrochloric acid, and incubated on ice for 30 min. After centrifugation at 11000 × *g* for 10 min, the supernatant fraction was dialyzed against 0.1 mol/liter acetic acid twice and against H_2O three times. After dialysis, the protein concentrations of extracts were measured, and equal aliquots of extracts were subjected to 18% SDS-PAGE. Western blotting for acetylated histone-3/4 and for total histone-3/4 was performed using goat anti-acetylated histone-3/4 polyclonal antibodies (Santa Cruz Biotechnology) and rabbit anti-histone-3/4 polyclonal antibodies (Santa Cruz Biotechnology), respectively.

Chromatin Immunoprecipitation Assay and Real-time PCR Analysis—Chromatin immunoprecipitation assays were performed as previously described (10) with the following modifications. In brief, after fixation of the genomic DNA and nuclear proteins with formalin, extracts were sonicated, subsequently immunoprecipitated with goat polyclonal anti-acetylated histone-4 antibody (Santa Cruz Biotechnology), goat polyclonal anti-GATA-4 antibody (Santa Cruz Biotechnology), or control goat IgG, and immunocomplexes were captured by adding protein G beads. After the precipitates were washed four times in the low stringency buffer, DNA was purified by phenol-chloroform extraction, and precipitated with ethanol. To detect the atrial natriuretic factor (ANF) promoter, which contains two GATA-4 sites (−281/−273 and −123/−118), collected DNA was subjected to real-time quantitative PCR analysis using a thermal cycler (ABI Prism®7900HT sequence detection system) with the detection probe and specific primers for the ANF promoter (−292/−93). Sequences of the primers were as follows: FAM-AATGTGACTCTTGCAGCTGAGGGTCTGG-TAMRA (detection probe; Applied Biosystems), 5′-GAGCGCCCAGGAAGATAACC-3′(sense for the ANF promoter), and 5′-GCCAGGAGAAGATGCCCTTT-3′(antisense for the ANF promoter).

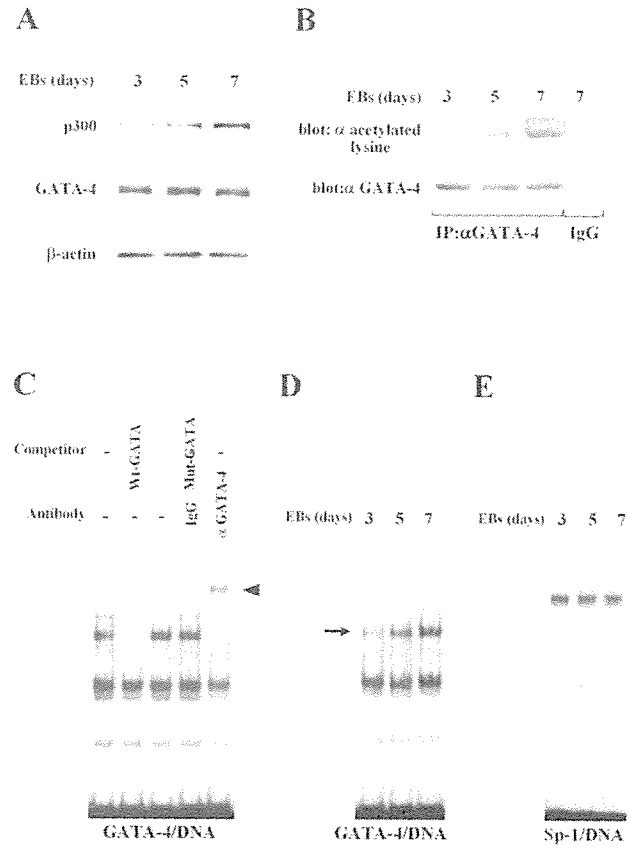

FIG. 1. **Acetylated form of GATA-4 and GATA-4/DNA binding increases in concert with expression of p300 during the differentiation of ES cells.** *A*, protein extracts from embryoid bodies (EBs days 3, 5, 7, respectively) were subjected to Western blotting for p300, GATA-4, and β-actin. *B*, the extracts (200 μg of protein) were immunoprecipitated with anti-GATA-4 antibody or IgG, followed by sequential Western blotting with anti-acetylated lysine antibody and anti-GATA-4 antibody. *C*, the extracts from EBs (day 7) were probed with a radiolabeled double-stranded oligonucleotide containing the GATA site. Unlabeled competitor DNAs were present at a 100-fold molar excess where indicated. *Lane 2*, a wild-type GATA oligonucleotide (*Wt-GATA*); *lane 3*, a mutant GATA oligonucleotide (*Mut-GATA*). Supershift assays were performed in the presence of 4 μg of either anti-GATA-4 antibody or IgG as indicated (*lanes 4 and 5*). *D* and *E*, the amounts of GATA-4/DNA binding (*D*) and Sp-1/DNA binding (*E*) were compared among the same extracts used for *panels A* and *B*.

Immunocytochemistry and Western Blotting for Cardiac Myosin Heavy Chain—After EBs were incubated with trypsin-EDTA, the cells were dissociated, resuspended in the medium, and grown in flask-style chambers with human fibronectin-coated slides (BD Biosciences). After a 24-h incubation, cells were subjected to immunocytochemistry for β-myosin heavy chain (MHC) as previously described (11). Briefly, after fixation the cells were incubated with anti-cardiac β-MHC monoclonal antibody (Novocastra Laboratories) at a dilution of 1:50, followed by incubation with anti-mouse horseradish peroxidase-conjugated secondary antibody (Jackson ImmunoResearch) at a dilution of 1:200. 30 μg of whole cell lysates extracted from EBs were subjected to Western blotting using anti-cardiac MHC monoclonal antibody that reacts with both α- and β-cardiac MHC. The levels of signals were quantified by densitometry using NIH image1.61.

Flow Cytometry—For the quantitative analysis of the number of GFP-positive cells in Nkx2.5-GFP ES cells, EBs were dissociated into single cells and analyzed by flow cytometry (BD Biosciences) as previously described (9).

Gene Expression Analysis by Real-time RT-PCR—Total RNA was isolated from EBs by using TRIzol® reagent (Invitrogen). RNA samples were treated with DNaseI (Invitrogen) to eliminate genomic DNA contamination, and cDNA was synthesized by using SuperScriptTMII reverse transcriptase (Invitrogen). For real-time PCR, the reaction was performed with a SYBR® Green PCR master mix (Applied Biosystems),

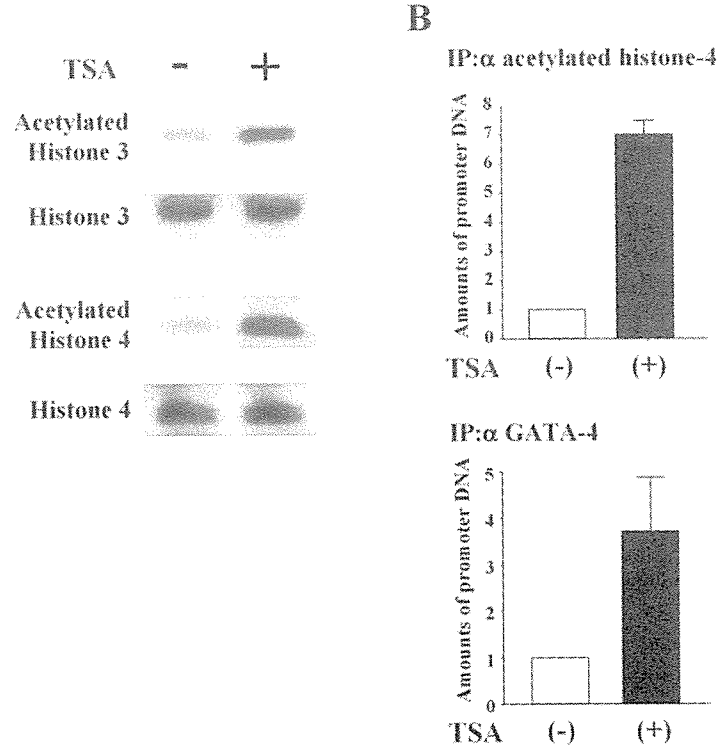

FIG. 2. **Analysis of histone acetylation and GATA-4/DNA binding induced by trichostatin A (*TSA*).** *A*, EBs (day 7) were stimulated with TSA (10 ng/ml) for 24 h. Proteins from the EBs were then isolated by acid extraction and subjected to Western blotting for acetylated histone-3/4 and histone-3/4 as indicated. *B*, EBs stimulated with TSA (10 ng/ml) for 24 h (days 7–8) were subjected to chromatin immunoprecipitation followed by quantification by real-time PCR. After fixation by formalin, chromatin from EBs was immunoprecipitated with anti-acetylated histone-4 antibody. ANF promoter sequences (−292/−93) including two GATA elements (−281/−273 and −123/−118) were detected by real-time PCR analysis. A graphic presentation of results obtained by real-time PCR is shown. The amount of PCR product amplified from untreated EBs was set at 1.0 in each experiment. Data are presented as the means ± S.E. of three independent experiments.

and the products were analyzed with a thermal cycler (ABI Prism®7900HT sequence detection system). Levels of GAPDH transcript were used to normalize cDNA levels. Gene-specific primers were used as previously described (9).

Statistical Analysis—Data are presented as means ± S.E. Statistical comparisons were performed using unpaired two-tailed Student's *t* tests or analysis of variance with Scheffe's test where appropriate, with a probability value <0.05 taken to indicate significance.

RESULTS

Expression of p300 and the Acetylated Form of GATA-4 Concomitantly Increases during the Differentiation of ES Cells into Cardiac Myocytes—We examined the time dependence of the expression of p300 and GATA-4 proteins during the differentiation of ES cells into cardiac myocytes. The day on which EBs were transferred into Petri dishes was set as day 0. The expression level of GATA-4 was almost constant on days 3, 5, and 7, though the level slightly increased from day 3 to day 5 (Fig. 1*A*, *middle panel*). In contrast, p300 expression progressively increased from day 3 to day 7 (Fig. 1*A*, *upper panel*). The expression level of β-actin was almost constant. As p300 is able to acetylate GATA-4, we examined whether the acetylated form of GATA-4 also increased in a time-dependent manner during the ES cell differentiation. Protein extracts from EBs at days 3, 5, and 7 were subjected to immunoprecipitation with an anti-GATA-4 antibody, followed by Western blotting using anti-acetylated lysine antibody. As shown in Fig. 1*B*, *upper panel*, the acetylated form of GATA-4 progressively increased from day 3 to day 7, consistent with the expression pattern of p300. The anti-acetylated lysine antibody was stripped, and then the membrane was reprobed with the anti-GATA-4 antibody. GATA-4 was similarly immunoprecipitated with anti-GATA-4 antibody in these three groups (Fig. 1*B*, *lower panel*). No protein was immunoprecipitated with control IgG (*lane four*).

GATA-4/DNA Binding Increases Concomitantly with GATA-4 Acetylation during ES Cell Differentiation—Next, to examine the changes in the DNA binding activity of GATA-4 during ES cell differentiation, EMSAs were performed. The same extracts from EBs used to detect acetylation were probed with a radiolabeled double-stranded oligonucleotide containing a GATA site. As shown in Fig. 1*C*, competition EMSAs demonstrated that the retarded band represented specific binding, as evidenced by the fact that it was competed out by an excess of unlabeled GATA oligonucleotide (*lane 2*) but not by the same amount of an oligonucleotide containing a GATA site with a mutation (*lane 3*). Furthermore, the retarded band was supershifted by anti-GATA-4 antibody (*lane 5*) but not by control goat IgG (*lane 4*). These data confirm that the retarded band represents an interaction of the probe with GATA-4. The amount of GATA-4/DNA binding (Fig. 1*D*) was markedly increased from day 3 to day 7, whereas Sp-1/DNA binding (Fig. 1*E*) was not altered. This was consistent with the increase in the amounts of p300 and acetylated GATA-4.

An HDAC Inhibitor, TSA, Induces Acetylation of Histone Tails and Increases the Accessibility of GATA-4 to the ANF Promoter—To examine the effect of TSA, a specific HDAC inhibitor, on the differentiation of ES cells, we first determined whether TSA treatment induces the acetylation of histone tails in these cells. Seven days after the transfer of EBs onto Petri dishes, ES cells were stimulated with TSA for 24 h. Protein extracts from these cells were then subjected to immunoblotting for the acetylated states of histone-3 and histone-4. As shown in Fig. 2*A*, TSA treatment of ES cells enhanced the acetylation of both histone-3 and histone-4. GATA-4 binds two GATA elements (−281/−273 and −123/118) within the ANF promoter and activates this promoter in a sequence-specific manner (12). As GATA-4 is a substrate of an intrinsic HAT, p300, using chromatin immunoprecipitation assays we examined whether histones near GATA-4 sites within the ANF promoter are acetylated as a result of TSA treatment and, if so, whether the treatment increases the accessibility of GATA-4 to the ANF promoter. Before immunoprecipitation, input genomic DNA was measured using GAPDH primers (Applied Biosystems) by comparison with the standard curve shown in supplemental Fig. S1*A*, *left panels*. Extracts from non-treated and TSA-treated ES cells containing the same amounts of GAPDH

were immunoprecipitated with anti-acetylated histone-4 antibody, anti-GATA-4 antibody, or with control goat IgG as a negative control. DNA was then purified from these precipitates and subjected to real-time PCR to quantify the amount of GATA-4 site-containing DNA sequences in the ANF promoter. We quantified the amounts of DNA by comparison with the standard curve shown in supplemental Fig. S1A, *right panels*. As shown in Fig. 2*B*, in extracts precipitated with anti-acetylated histone-4 antibody and those precipitated with anti-GATA-4 antibody, the amount of the ANF promoter containing two GATA-4 sites was much higher in TSA-treated ES cells than in non-treated ES cells. However, this promoter was not detectable in the extracts precipitated with IgG. These findings demonstrate that treatment of ES cells with TSA induces acetylation of histones near GATA-4 sites within the ANF promoter and increases the accessibility of GATA-4 to these sites.

TSA Induces Acetylation of GATA-4 and Enhances GATA-4/DNA Binding in ES Cells—We next examined whether TSA also induces acetylation of the DNA binding transcription factor GATA-4 in ES cells. On day 7, ES cells were stimulated with TSA for 24 h, pulse-labeled with [^{14}C]acetic acid sodium salt, and subjected to immunoprecipitation with antiserum against GATA-4 or with control goat IgG as a negative control. As shown in Fig. 3*A*, *upper panel*, incorporation of sodium [^{14}C]acetate into GATA-4 protein was increased by TSA treatment. TSA-induced acetylation of GATA-4 was also confirmed by immunoprecipitation with anti-GATA-4 antibody followed by Western blotting with anti-acetylated-lysine antibody (Fig. 3*A*, *middle panel*). After the anti-acetylated lysine antibody was stripped, the membrane was reprobed with the anti-GATA-4 antibody. GATA-4 was similarly immunoprecipitated with anti-GATA-4 antibody in non-treated and TSA-treated cell extracts (Fig. 3*A*, *lower panels*). No protein was immunoprecipitated with control IgG (*lane 3*). These results indicate that TSA augments the acetylation of GATA-4 in ES cells. As shown in Fig. 3*B*, the expression of p300 was also increased by TSA stimulation, whereas the levels of GATA-4 and β-actin expression were almost constant. In addition, we performed EMSAs using protein extracts from ES cells to determine whether TSA treatment increased the DNA binding of GATA-4. We confirmed by competition and supershift assays that the retarded band indicated by the *arrow* in Fig. 3*C* represents specific binding of the probe with GATA-4, similar with the findings shown in Fig. 1*C*. The GATA-4/DNA binding was increased by TSA treatment in ES cells (Fig. 3*C*), whereas Sp-1/DNA binding was not altered by TSA treatment (Fig. 3*D*).

TSA Promotes the Differentiation of ES Cells into Cardiac Myocytes—Finally, to determine whether TSA promotes the differentiation of ES cells into cardiac myocytes, we utilized an ES cell line (Nkx2.5-GFP ES cells) that expresses GFP under the transcriptional control of the cardiac-specific Nkx2.5 promoter. The cardiac specificity of GFP-positive cells in this cell line was shown in a previous study (9). In agreement with a previous study, we confirmed by cell sorting and immunocytochemistry for β-MHC that more than 90% of GFP-positive cells were positive for β-MHC and that none of the GFP-negative cells was β-MHC-positive (data are not shown). EBs derived from Nkx2.5-GFP ES cells (day 7) were stimulated with TSA (10 ng/ml) for 24 h. As shown in Fig. 4*A*, TSA-stimulated EBs showed distinct fluorescence, whereas non-stimulated EBs showed only vague fluorescence. Then we dissociated EBs, cultured the cells on the fibronectin-coated slides for 24 h, and stained them with an antibody against cardiac β-MHC. As shown in Fig. 4*B*, cells with brown signals indicating the presence of β-MHC were observed predominantly in TSA-stimulated ES cells. For quantification, the cells dissociated from EBs were also subjected to flow cytometric analysis. In Fig. 4*C*, the *X*- and *Y*-axes in the dot blot represent GFP and propidium iodide (PI) signals, respectively. The percentage of GFP-positive ES cells was significantly ($p < 0.05$) increased by TSA treatment. TSA did not affect the number of propidium iodide-positive cells, excluding the possibility of its nonspecific toxic effects on ES cells.

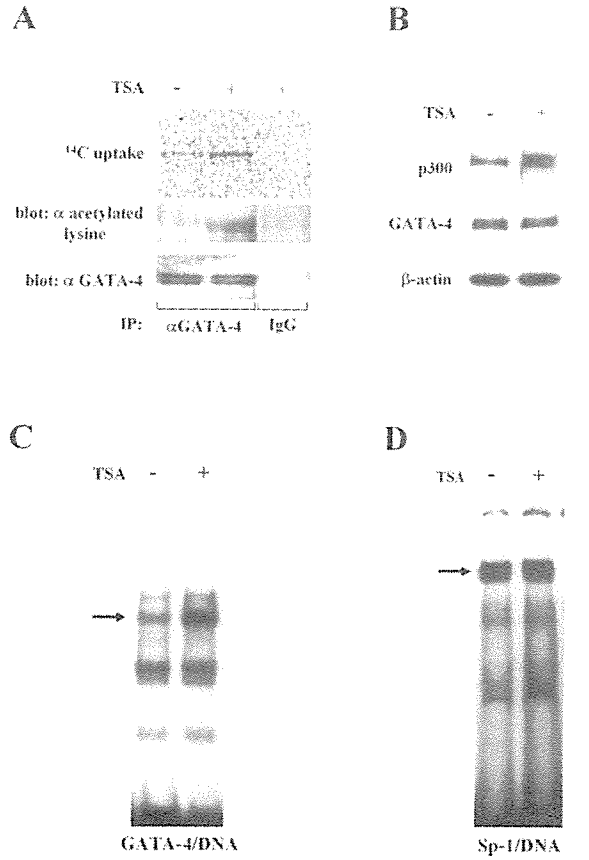

FIG. 3. **Trichostatin A (*TSA*) induces acetylation and DNA binding of GATA-4 in EBs.** *A*, EBs were stimulated with TSA (10 ng/ml) for 24 h (days 7–8) and were pulse-labeled with [^{14}C]acetic acid sodium salt for 3 h. Protein extracts were immunoprecipitated with anti-GATA-4 antibody or with control goat IgG, resolved by sodium dodecyl sulfate (SDS)-polyacrylamide gel electrophoresis, fixed, and autoradiographed using a bioimaging analyzer (*upper panel*). The same extracts (200 μg of protein) were immunoprecipitated with anti-GATA-4 antibody, followed by sequential Western blotting with anti-acetylated lysine antibody (*middle panel*) and with anti-GATA-4 antibody (*lower panel*). *B*, the extracts used for *panel A* before immunoprecipitation were subjected to Western blotting using the anti-p300 antibody (*upper panel*), anti-GATA-4 antibody (*middle panel*), and anti-β-actin antibody (*lower panel*). *C* and *D*, the same nuclear extracts were probed with a radiolabeled double-stranded oligonucleotide containing the GATA-4 site (*C*) and with one containing the Sp-1 site (*D*).

To confirm that TSA directs differentiation of ES cells into cardiac myocytes, we performed quantitative RT-PCR analysis using specific primers for the detection of mRNAs encoding Nkx2.5 and ANF. After total RNA was extracted from EBs (days 7–8) incubated with or without TSA for 24 h, cDNA was synthesized and subjected to real-time PCR. The amounts of cDNA for the Nkx2.5, ANF, and GAPDH genes were measured by comparison with the respective standard curves (supplemental Fig. S1*B*). Consistent with the data of flow cytometry, the mRNA levels of Nkx2.5 and ANF were increased by TSA treatment, as shown in Fig. 5*A*. Furthermore, whole cell lysates extracted from EBs treated with or without TSA for 48 h (days

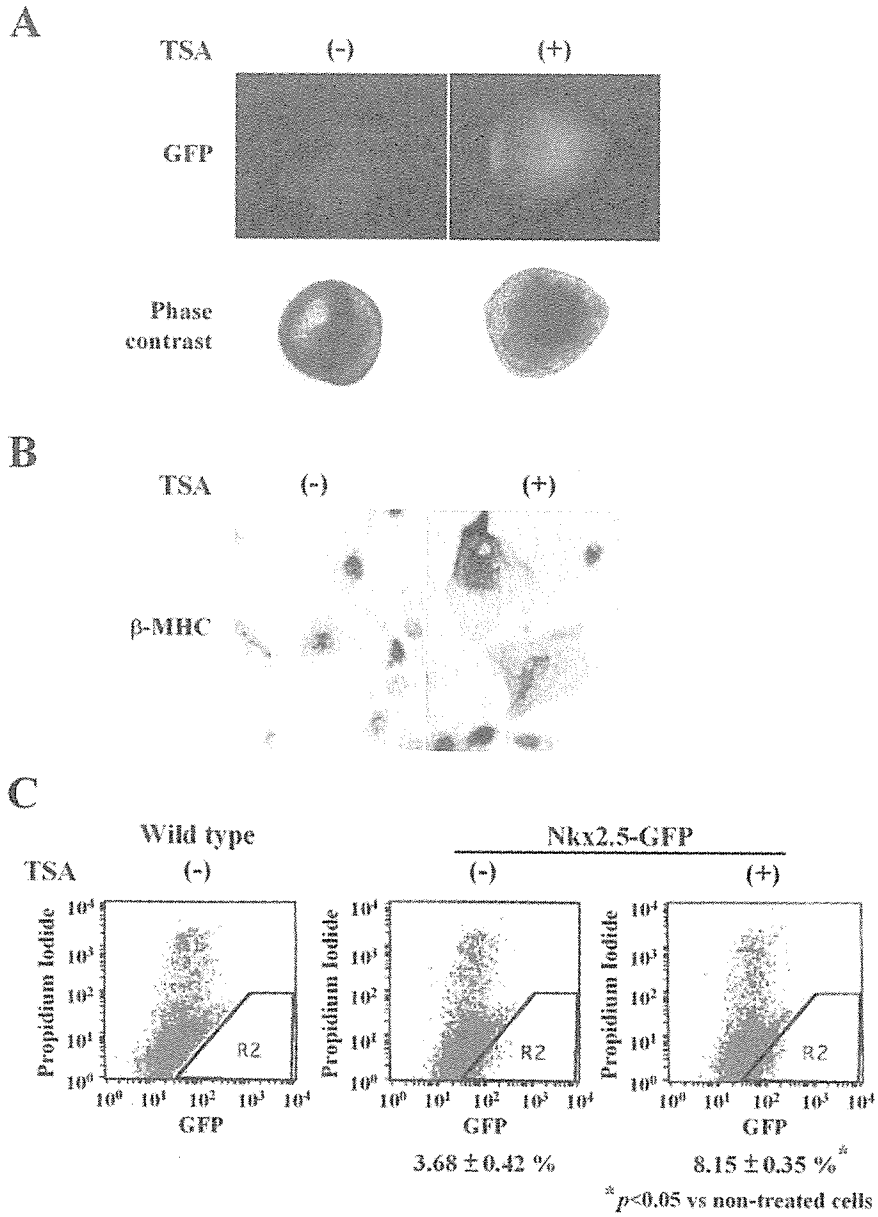

FIG. 4. **Trichostatin A (*TSA*) promotes the differentiation of ES cells into cardiac myocytes.** *A*, EBs were stimulated with TSA (10 ng/ml, *right panels*) or incubated without treatment (*left panels*) for 24 h (days 7–8). Representative EBs showing green fluorescent protein (*GFP*) signals were observed through a fluorescence microscope (*upper panels*). *B*, these EBs were then dissociated into single cells, recultured on fibronectin-coated slides for 24 h, and subjected to immunocytochemistry for β-myosin heavy chain (*β-MHC*). *C*, EBs were stimulated with TSA (10 ng/ml) for 24 h (days 7–8), dissociated into single cells, and subjected to flow cytometric analysis for the detection of GFP-positive cells. The *X*- and *Y*-axes show the intensity of GFP fluorescence and propidium iodide fluorescence, respectively. The percentage of GFP-positive cells was calculated. Data are presented as the means ± S.E. of three independent experiments.

7–9) were subjected to Western blotting for cardiac MHC. TSA increased protein expression of cardiac MHC (Fig. 5*B*). These findings suggest that TSA treatment promotes the differentiation of ES cells into cardiac myocytes.

DISCUSSION

Differentiation of ES cells into cardiac myocytes requires activation of a cardiac-specific gene program. HATs and HDACs are profoundly involved in gene expression by modulating acetylation of specific transcription factors as well as of histones. The present study was performed to examine the roles of nuclear acetylation during the ES cell differentiation into cardiac myocytes.

Several lines of evidence suggest that p300 is critical for the development of the embryonic heart. Expression of p300 is relatively abundant in the heart, begins to be detected as early as embryo day 7.5, and increases during the subsequent developmental stages (13, 14). Homozygous p300 knock-out mice die between 9 and 11.5 days of gestation, exhibiting defects in proper heart development (13). p300 acts as a transcriptional coactivator of GATA-4, one of the earliest markers of cardiac myocyte differentiation, and is required for cardiac-specific gene expression (12, 15). In addition, p300 is able to acetylate GATA-4 and enhance its DNA binding activity (8). Homozygous mice in which HAT mutant p300 is knocked in exhibit developmental defects similar to those in p300 knock-out mice (16). These findings demonstrate that the HAT activity of p300 is required for proper heart development. The present study demonstrated that the acetylated form of GATA-4 and GATA-4/DNA binding increases in concert with the expression level of p300 during the differentiation of ES cells into cardiac myocytes. These findings suggest that p300 is involved in increasing the acetylation and DNA binding of GATA-4 during myocardial cell differentiation, while the precise roles of p300 HAT activity should be clarified by further studies.

Acetylation of nuclear proteins is also regulated by HDACs, whose functions are opposed by HATs (4, 17). HDACs repress gene expression not only by affecting chromatin structure but also by directly acting on transcriptional activators, co-repressors, and DNA binding factors. HDACs directly interact with DNA binding transcription factors such as p53, MyoD, and

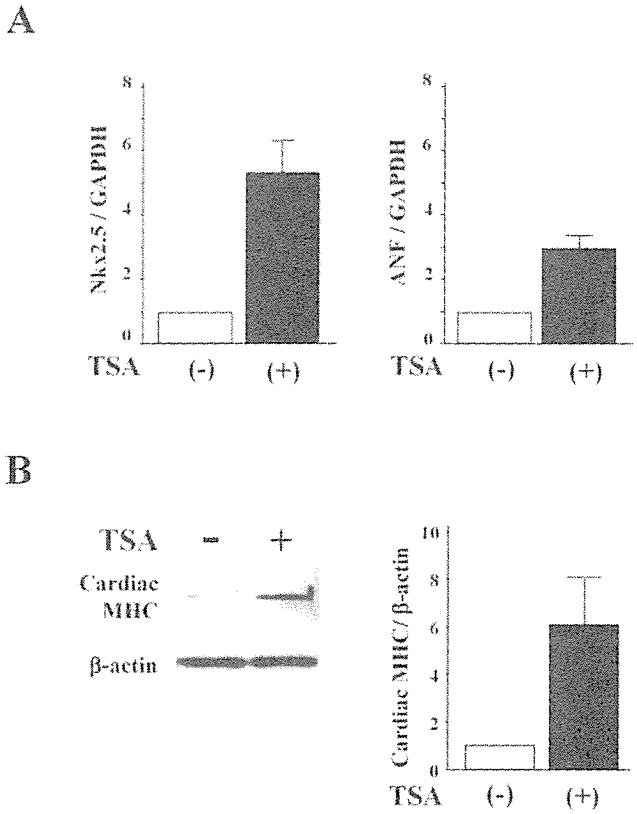

FIG. 5. **Trichostatin A (*TSA*) increased the expression of cardiac genes in EBs.** *A*, EBs were incubated with or without TSA (10 ng/ml) for 24 h (days 7–8). Total RNA was extracted, and synthesized cDNA was subjected to real-time PCR. The amounts of cDNA for the Nkx2.5, atrial natriuretic factor (*ANF*), and GAPDH genes were measured. Levels of GAPDH transcript were used to normalize cDNA levels. The amount of PCR product amplified from untreated EBs was set at 1.0 in each experiment. Data are presented as the means ± S.E. of three independent experiments. *B*, EBs were incubated with or without TSA (10 ng/ml) for 48 h (days 7–9). Whole cell lysates extracted from EBs were subjected to Western blotting for cardiac myosin heavy chain (*MHC*) and β-actin. *Left panels* show representative photographs. In the *right graph*, results of quantitative analysis of Western blotting are expressed as means ± S.E. of three independent experiments.

myocyte enhancing factor 2, deacetylate these factors, and repress their transcriptional activity (18–20). HDACs also perturb the interaction between HATs (p300/cAMP-response element-binding protein-binding protein) and their target transcription factors. Furthermore, HDACs are able to recruit other transcriptional co-repressors to the target genes (17, 21). In agreement with previous reports, the present study demonstrated that inhibition of HDACs by TSA induced acetylation of histone tails in ES cells (22, 23). These tails included GATA-4 site-containing DNA sequences within the ANF promoter. In addition, TSA enhanced the acetylation of GATA-4 during the differentiation of ES cells into cardiac myocytes. These findings suggest that post-translational GATA-4 modification as well as epigenetic modification are involved in the increase in GATA-4/DNA binding. The results also suggest the hypothesis that TSA treatment releases HDACs from GATA-4 and promotes interaction between p300 and GATA-4. However, TSA also increased the amount of p300 protein in ES cells. Further studies are needed to clarify the precise mechanisms by which TSA induces acetylation and DNA binding of GATA-4.

The present study demonstrated that TSA promotes the differentiation of ES cells into cardiac myocytes. In contrast, it has been reported that TSA inhibits the differentiation of adipocytes (22) or oligodendrocytes (23). In the skeletal muscle cell lineage, TSA either augments or inhibits the differentiation depending on the developmental stage (24). These findings suggest that TSA has differential effects in distinct cell types or developmental stages. In addition, individual HDACs play differential roles in cardiac myocytes. For example, one of the class II HDACs, HDAC9, represses the pro-hypertrophic gene program, whereas class I HDAC seems to suppress anti-hypertrophic gene expression (25–27). Therefore, further studies are needed on the role of each HDAC in different stages of ES cell differentiation into cardiac myocytes.

We have shown here that acetylation of GATA-4 as well as of histones occurs during the differentiation of ES cells into cardiac myocytes and that further augmentation of the acetylation by TSA promotes the differentiation. It is unclear at present whether acetylation of GATA-4 in whole EBs represents acetylation of GATA-4 in cardiac myocytes or their precursors. In mouse embryogenesis, however, GATA-4 is expressed in cardiac tissue during formation and bending of the heart tube at day 8 postcoitum (28). In contrast, GATA-4 is expressed later in the gut epithelium and in primitive gonads (at around day 11.5 postcoitum) (29, 30). These findings suggest that GATA-4 expression is restricted to cardiac tissue during early stages of heart development. Therefore, acetylation of GATA-4 detected in the entire EBs might represent acetylation of cardiac GATA-4, which possibly contributes to the differentiation of ES cells into cardiac myocytes. These findings emphasize the important roles of nuclear acetylation in myocardial cell differentiation. Our findings might be applicable to the differentiation of endogenous stem cells into cardiac myocytes *in vivo*. At present, the differentiation efficiency is too low to be used for myocardial regeneration therapy for patients with end-stage heart failure. Therefore, it would be interesting to test the usefulness of TSA for this therapy *in vivo*.

Acknowledgments—We thank N. Sowa and S. Nagata for excellent technical assistance.

REFERENCES

1. Sachnidis, A., Fleischmann, B. K., Kolossov, E., Wartenberg, M., Sauer, H., and Hescheler, J. (2003) *Cardiovasc. Res.* **58,** 278–291
2. Grepin, C., Nemer, G., and Nemer, M. (1997) *Development* **124,** 2387–2395
3. Chan, H. M., and La Thangue, N. B. (2001) *J. Cell Sci.* **114,** 2363–2373
4. Johnson, C. A., and Turner, B. M. (1999) *Semin. Cell Dev. Biol.* **10,** 179–188
5. Shikama, N., Lyon, J., and Thangue, N. B. (1997) *Trends Cell Biol.* **7,** 230–236
6. Gu, W., Shi, X. L., and Roeder, R. G. (1997) *Nature* **387,** 819–823
7. Lill, N. L., Grossman, S. R., Ginsberg, D., DeCaprio, J., and Livingston, D. M. (1997) *Nature* **387,** 823–827
8. Yanazme, T., Hasegawa, K., Morimoto, T., Kawamura, T., Wada, H., Matsumori, A., Kawase, Y., Hirai, M., and Kita, T. (2003) *Mol. Cell. Biol.* **23,** 3593–3606
9. Hidaka, K., Lee, J. K., Kim, H. S., Ihm, C. H., Iio, A., Ogawa, M., Nishikawa, S., Kodama, I., and Morisaki, T. (2003) *FASEB J.* **17,** 740–742
10. Ferreira, R., Naguibneva, I., Mathieu, M., Ait-Si-Ali, S., Robin, P., Pritchard, L. L., and Harel-Bellan, A. (2001) *EMBO Rep.* **2,** 794–799
11. Yanazume, T., Hasegawa, K., Wada, H., Morimoto, T., Abe, M., Kawamura, T., and Sasayama, S. (2002) *J. Biol. Chem.* **277,** 8618–8625
12. Kakita, T., Hasegawa, K., Morimoto, T., Kaburagi, S., Wada, H., and Sasayama, S. (1999) *J. Biol. Chem.* **274,** 34096–34102
13. Yao, T. P., Oh, S. P., Fuchs, M., Zhou, N. D., Ch'ng, L. E., Newsome, D., Bronson, R. T., Li, E., Livingston, D. M., and Eckner, R. (1998) *Cell* **93,** 361–372
14. Partanen, A., Motoyama, J., and Hui, C. C. (1999) *Int. J. Dev. Biol.* **43,** 487–494
15. Dai, Y. S., and Markham, B. E. (2001) *J. Biol. Chem.* **276,** 37178–37185
16. Shikama, N., Lutz, W., Kretzschmar, R., Sauter, N., Roth, J-F., Marino, S., Wittwer, J., Scheidweiler, A., and Eckner, R. (2003) *EMBO. J.* **22,** 5175–5185
17. Jenuwein, T., and Allis, C.D. (2001) *Science* **293,** 1074–1080
18. Luo, J., Su, F., Chen, D., Shiloh, A., and Gu, W. (2000) *Nature* **408,** 377–381
19. Mal, A., Sturniolo, M., Schiltz, R. L., Ghosh, M. K., and Harter, M. L. (2001) *EMBO J.* **20,** 1739–1753
20. McKinsey, T. A., Zhang, C. L., and Olson, E. N. (2001) *Curr. Opin. Genet. Dev.* **11,** 497–504
21. Khochbin, S., Verdel, A., Lemercier, C., and Seigneurin-Berny, D. (2001) *Curr. Opin. Genet. Dev.* **11,** 162–166
22. Lagace, D. C., and Nachtigal, M. W. (2004) *J. Biol. Chem.* **279,** 18851–18860
23. Marin-Husstege, M., Muggironi, M., Liu, A., and Casaccia-Bonnefil, P. (2002) *J. Neurosci.* **22,** 10333–10345

24. Iezzi, S., Cossu, G., Nervi, C., Sartorelli, V., and Puri, P. L. (2002) *Proc. Natl. Acad. Sci. U. S. A.* **99,** 7757–7762
25. Zhang, C. L., McKinsey, T. A., Chang, S., Antos, C. L., Hill, J. A., and Olson, E. N. (2002) *Cell* **110,** 479–488
26. Kook, H., Lepore, J. J., Gitler, A. D., Lu, M. M., Wing-Man Yung, W., Mackay, J., Zhou, R., Ferrari, V., Gruber, P., and Epstein, J. A. (2003) *J. Clin. Investig.* **112,** 863–871
27. Hamamori, Y., and Schneider, M. D. (2003) *J. Clin. Investig.* **112,** 824–826
28. Heikinheimo, M., Scandrett, J. M., and Wilson, D. B. (1994) *Dev. Biol.* **164,** 361–373
29. Laverriere, A. C., MacNeill, C., Mueller, C., Poelmann, R. E., Burch, J. B., and Evans, T. (1994) *J. Biol. Chem.* **269,** 23177–23184
30. Viger, R. S., Mertineit, C., Trasler, J. M., and Nemer, M. (1998) *Development* **125,** 2665–2675

STEM CELLS®
Original Article

Two Different Roles of Purified CD45$^+$c-Kit$^+$Sca-1$^+$Lin$^-$ Cells After Transplantation in Muscles

MOMOKO YOSHIMOTO,[a] HSI CHANG,[a] MITSUTAKA SHIOTA,[a] HIROHIKO KOBAYASHI,[a] KATSUTSUGU UMEDA,[a] ATSUSHI KAWAKAMI,[b] TOSHIO HEIKE,[a] TATSUTOSHI NAKAHATA[a]

[a]Department of Pediatrics, Graduate School of Medicine, Kyoto University, Kyoto, Japan;
[b]Department of Biological Science, Graduate School of Sciences, University of Tokyo, Tokyo, Japan

Key Words. Hematopoietic stem cells • Transplantation • c-Kit$^+$Sca-1$^+$Lin$^-$ • Muscle stem cells

ABSTRACT

Recent studies have indicated that bone marrow cells can regenerate damaged muscles and that they can adopt phenotypes of other cells by cell fusion. Our direct visualization system gave evidence of massive muscle regeneration by green fluorescent protein (GFP)–labeled CD45$^+$c-Kit$^+$Sca-1$^+$Lin$^-$ cells (KSL cells), and we investigated the role of KSL cells in muscle regeneration after transplantation with or without lethal irradiation. In the early phase, GFP signals were clearly observed in all the muscles of only irradiated mice. Transverse cryostat sections showed GFP$^+$myosin$^+$ muscle fibers, along with numerous GFP$^+$ hematopoietic cells in damaged muscle. These phenomena were temporary, and GFP signals had dramatically reduced 30 days after transplantation. After 6 months, GFP$^+$ fibers could hardly be detected, but GFP$^+$c-Met$^+$ mononuclear cells were located beneath the basal lamina where satellite cells usually exist in both conditioned mice. Immunostaining of isolated single fibers revealed GFP$^+$PAX7$^+$, GFP$^+$MyoD$^+$, and GFP$^+$Myf5$^+$ satellite-like cells on the fibers. Single-fiber cultures from these mice showed proliferation of GFP$^+$ fibers. These results indicate two different roles of KSL cells: one leading to regeneration of damaged muscles in the early phase and the other to conversion into satellite cells in the late phase. STEM CELLS *2005;23:610–618*

INTRODUCTION

Various tissue-specific stem cells have been identified in epidermis [1], intestinal epithelium [2], testis [3], liver [4], brain [5], and muscle [6]. Until recently, it was thought that tissue-specific stem cells could only differentiate into their original tissue, but it has been demonstrated that they can also differentiate into other lineages. For example, cells of donor origin have been detected in liver, heart, vascular endothelium, skeletal muscles, and other organs after bone marrow (BM) transplantation [7–14]. Of special interest for our study is that BM-derived cells have been shown to participate in the regeneration of chemically damaged fibers in skeletal muscle [12]. Subsequent studies showed that dystrophin-positive myofibers were restored in mdx mice, an animal model of Duchenne's muscular dystrophy, after transplantation of stem cells purified by fluorescence-activated cell sorting with Hoechst 33342 low-stained cells, also known as side population (SP) cells [15]. In short, stem cells in BM, comprising hematopoietic stem cells (HSCs) and mesenchymal stem cells (MSCs), have been found to be capable of regenerating damaged muscle fibers after BM transplantation.

It has also been demonstrated, however, that BM cells can adopt the phenotype of other cells by means of cell fusion [16, 17]. These investigators warned that in vivo "transdifferentiation" might result from cell fusion. The differentiation potential of BM cells beyond the lineage restriction of stem cells remains to be determined.

Correspondence: Tatsutoshi Nakahata, M.D., Ph.D., Department of Pediatrics, Graduate School of Medicine, Kyoto University, 54 Kawahara-cho, Shogoin, Sakyo-ku, Kyoto 606-8507, Japan. Telephone: 81-75-751-3290; Fax: 81-75-752-2361; e-mail: tnakaha@kuhp.kyoto-u.ac.jp Received September 2, 2004; accepted for publication January 13, 2005. 1066-5099/2005/$12.00/0 doi: 10.1634/stemcells.2004-0220

In addition to BM cells, SP cells have also been identified in muscle tissues [15, 18]. These muscle SP cells are reported to have hematopoietic as well as myogenic potential [19] and to express CD45 antigen, which is recognized as a hematopoietic cell marker. Another study gave evidence that $CD45^+$ cells in skeletal muscle are of BM origin [20]. These reports thus indicate that hematopoietic cells of BM origin seem to be present in skeletal muscles. However, the correlations among HSCs, $CD45^+$ cells in skeletal muscle, satellite cells, myogenic precursors, and muscle-derived stem cells have not yet been determined. It is important to clarify these relationships, both for scientific research and for the application of stem cell therapy.

To investigate the potential and the kinetics of HSCs in skeletal muscles, we transplanted $c\text{-}Kit^+Sca\text{-}1^+Lin^-$ (KSL) cells as enriched HSC fraction from green fluorescent protein (GFP) transgenic mice into lethally irradiated C57BL/6 mice or nonirradiated W/W^v neonates that can accept HSCs without myeloablation. We examined the time-course behavior of GFP^+ cells in recipient muscles with a fluorescent stereomicroscope and immunohistochemical staining during the early and late phases after transplantation. Our visualization system makes it possible to detect transplanted cells with GFP signals in intact organs without the need to make sections first and can easily trace their kinetics throughout the entire body [21]. With this system, we found that myeloablation enables KSL cells to migrate into damaged muscles and to regenerate muscle fibers in the whole body during the early phase following transplantation. In the late phase, progenies of KSL cells had remained in muscle tissues and gave rise to satellite cells with myogenic potential, regardless of whether the mice had been irradiated.

Materials and Methods

Mice

Pregnant female W/+ mice mated with W^v/+ mice were obtained from Shizuoka Laboratory Animal Center (Shizuoka, Japan). GFP transgenic mice were kindly provided by Dr. M. Okabe (Osaka University, Japan). The background of all these mice was C57BL/6. All cells except erythrocytes of transgenic mice expressed GFP protein. The mice were bred and maintained in a specific pathogen-free microisolator environment. Neomycin in acidic water was supplied to irradiated recipient adult mice during the first month after transplantation.

Cell Sorting

BM cells were labeled with a cocktail of biotinated primary antibodies for CD3 (145-2C11), B220/CD45R (RA3-6B2), Mac-1 (M1/70), Gr-1 (RB6-8C5), and TER119 (TR119). All antibodies were purchased from Pharmingen (San Diego, http://www.bdbiosciences.com/pharmingen). Lineage-negative (Lin^-) cells were obtained by auto-magnetic cell sorting (MACS; Militenyi Biotec, Bergisch Gladbach, Germany, http://www.miltenyibiotec.com), according to the manufacturer's instructions. Lin^- cells were then stained with phycoerythrin (PE)–conjugated anti-Sca-1 antibody and allophycocyanin (APC)–conjugated anti-c-Kit antibody. KSL cells were collected by cell sorting on a FACSVantage (Becton, Dickinson, San Jose, CA, http://www.bd.com). To confirm that KSL cells are all hematopoietic cells based on the expression of CD45 antigen, we stained Lin^- cells collected from wild-type C57BL/6 mice with fluorescein isothiocyanate (FITC)–conjugated anti-CD45 antibody, PE-conjugated anti-Sca-1 antibody, and APC-conjugated anti-c-Kit antibody.

Transplantation and Sequential Analysis

One to 5×10^3 of KSL cells with 2×10^5 Ly5.1 BM cells were injected into the tail vein of C57BL/6 adult mice that had received 9.0 Gy irradiation or into the orbital branch of the anterior facial vein of W/W^v neonates within 0–3 days after birth. On days 3, 10, 20, and 30 after transplantation, all muscles were observed under a fluorescent stereomicroscope (Leica, Heerbrugg, Switzerland, http://www.leica.com). At least five mice were analyzed in each time point.

Adherent Cell Culture

To see if KSL cells contain any mesenchymal cells, we cultured 1 to 5×10^3 per well of KSL cells with MesenCult Medium (Stem Cell Technologies, Vancouver, Canada, http://www.stemcell.com) in 24-well plates for 14 days.

Immunohistochemistry

Muscles were fixed with 4% paraformaldehyde, embedded in the optimal cutting temperature compound. Frozen sections of 7-μm thickness were mounted on silane-coated glass slides. For immunostaining of single-muscle fiber [22], fibers were fixed with 4% paraformaldehyde and were permeabilized with 0.5% (vol/vol) Triton X-100 phosphate-buffered solution (PBS). Rabbit or mouse anti-GFP (BD Biosciences Clontech, Palo Alto, CA, http://www.bdbiosciences.com/clontech/), rat anti-CD45 (Pharmingen), mouse anti-myosin (Zymed Laboratories, San Francisco, http://www.zymed.com), mouse anti-myogenin, mouse anti-MyoD1 (Dako, Carpinteria, CA, http://www.ump.com/dako.html), rabbit anti-c-Met, rabbit anti-Myf5 (Santa Cruz Biotechnology, Santa Cruz, CA, http://www.scbt.com), rabbit anti-laminin (Dako), and mouse-anti PAX7 (generated from mouse hybridoma [23]) were used as the primary antibodies. Either alkaline phosphatase (ALP)–conjugated anti-rabbit, Alexa488-conjugated anti-rabbit, Alexa350-conjugated anti-rabbit, streptavisin Alexa350 Cy3–conjugated anti-rat or anti-mouse, FITC-conjugated anti-rabbit or anti-mouse was used as the secondary antibody. Hematoxylin or Hoechst 33324 was used for nuclear staining. These samples were then examined under a fluorescent microscope (Olympus, Tokyo, http://

www.olympus-global.com), an AS-MDW (Leica), or a confocal microscope (Olympus). Photographs were obtained with an AxioCam (Carl Zeiss Vision GmbH, Hallbergmoos, Germany, http://www.zeiss.com) or an AS-MDW (Leica).

FISH Analysis

For the detection of GFP DNA in myonuclei of the tissues at 30 days and 6 months after transplantation, fluorescence in situ hybridization (FISH) analysis was done. GFP detection was made using a polymerase chain reaction (PCR) digoxigenin (DIG) probe synthesis kit (Roche, Basel, Switzerland, http://www.roche.com). Hybridization was done according to the instructions of in situ hybridization kit (Nippon Gene, Toyama, Japan, http://www.nippongene.jp). In brief, frozen sections were fixed in 100% ethanol, followed by incubation in 90%, 80%, 70%, and 50% ethanol. Sections were incubated in 50 μg/ml of proteinase K for 15 minutes at 37°C. The GFP probe was denatured at 95°C and added to each slide following incubation on a 95°C hotplate. The sections were hybridized overnight at 42°C in a humidified chamber. Sections were washed three times in 50% formamide in 2× sodium chloride/sodium citrate (SSC) prewarmed to 42°C, then in 0.1× SSC at 42°C. Sections were washed in PBS, and a hybridized GFP probe was detected using peroxidase-conjugated anti-DIG antibody (Dako), following tyramide signal amplification (PerkinElmer Life and Analytical Science, Inc., Boston, http://las.perkinelmer.com).

Single-Fiber Culture

Single muscle fibers were explanted in matrigel-coated plates, as described previously [24]. Briefly, the bilateral soleus muscles were removed from the animal and incubated in collagenase for 90 minutes at 37°C. Digested fibers were then carefully explanted onto matrigel-coated 24-well plates. A plating medium, consisting of 10% horse serum (HS) and 0.5% chick embryo extract (Gibco, Carlsbad, CA, http://www.invitrogen.com) in Dulbecco's modified Eagle's medium (DMEM; Sigma Chemical Corp., St. Louis, http://www.sigma-aldrich.com) was added. The medium was replaced on day 4 with a growth medium consisting of 20% fetal calf serum (FCS), 10% HS, and 1% chick embryo extract in DMEM, and on day 8 with a differentiation medium, consisting of 2% FCS, 10% HS, and 0.5% chick embryo extract in DMEM.

PCR Analysis

Total DNA was extracted with a Dneasy Tissue Kit (Qiagen, Valencia, CA, http://www1.qiagen.com) from the 24-well plates used for culturing single fibers from hind limb muscles 6 months after transplantation of KSL cells. The primers for GFP were (5'-3') CTG GTC GAG CTG GAC GGC GAC G and CAC GAA CTC CAG CAG GAC CAT G. For nested GFP they were ACA AGT TCA GCG TGT CCG GCG A and CTT CTC GTT GGG GTC TTT GCT C. The PCR cycle using AmpliTaq Gold (Applied Biosystems, Foster City, CA, http://www.appliedbiosystems.com) for the GFP or nested GFP primer comprised 8 minutes at 95°C, 35 cycles at 94°C for 30 seconds, at 64°C for 30 seconds, and at 72°C for 40 seconds, followed by 7 minutes at 72°C.

Results

KSL Cells Can Repair Muscle Damage in Early Phase After Transplantation

To investigate the process of settlement of donor hematopoietic cells into skeletal muscles, HSC fraction, KSL cells [25], derived from BM of GFP-transgenic mice, were transplanted into lethally irradiated adult mice by tail vein injection. The entire KSL cell fraction was hematopoietic and expressed CD45 (Fig. 1). The purity of KSL cells after sorting was 98%. To exclude the possibility of contamination of mesenchymal cells, we cultured 1 to 5 × 10^3 per well of KSL cells with MesenCult medium for 14 days. No adherent cells were observed (data not shown).

After transplantation, the muscles in the entire body were examined, first with a fluorescent stereomicroscope and then with immunohistochemical staining, to detect the GFP signals. On day 3 after transplantation, no GFP signals could be detected in any muscles. On days 10 and 20, powerful GFP signals in

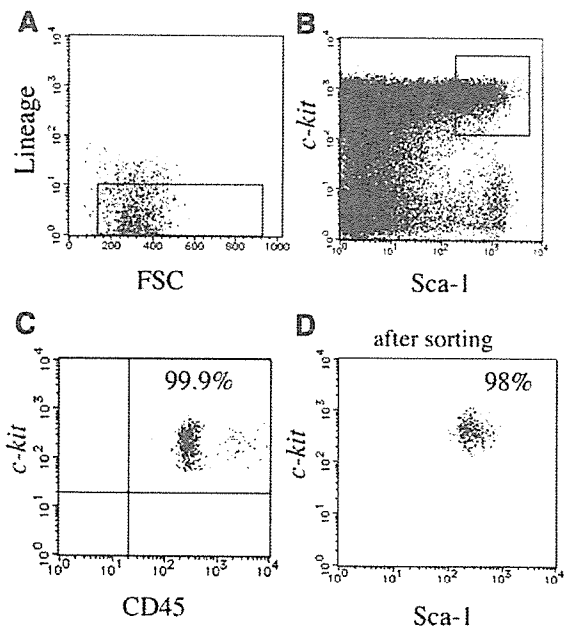

Figure 1. Purification of KSL cells. After collecting Lin^- cells by auto-MACS, KSL cells were sorted by FACSVantage. **(A):** Lin^- gating. **(B):** Sorting gate for KSL cells. **(C):** All KSL gated cells express CD45. **(D):** The purity of KSL cells after sorting was 98%. Abbreviation: FSC, forward scatter.

the muscle fibers throughout the body were observed under a fluorescent stereomicroscope such as in the intercostal, thigh, abdominal, greater pectoral, and external ocular muscles (Fig. 2A). Transverse sections showed muscle fibers of variable sizes with centrally localized nuclei, which represents the regenerative status (Fig. 2B). Among these muscle fibers, GFP$^+$ region–like muscle fibers were detected (Fig. 2B, b, arrowheads; faintly red region). There were mainly two types of GFP$^+$ regions. One region consisted of GFP$^+$ fibers (Fig. 3B), which were confirmed by typical cross-striations (Fig. 3A) and by immunostaining with anti-myosin antibody (Fig. 3C, D). And the other consisted of GFP$^+$ mononuclear cells (Fig. 3E), most of which were not stained with anti-myosin (Fig. 3G, H) but stained with anti-CD45 antibody (Fig. 3F, H). In the region of GFP$^+$ fibers, myogenin$^+$ myoblasts or myotubes were detected around the fibers (Fig. 4D, E, arrowheads). Interestingly, CD45^{low}myogenin$^+$GFP$^+$ cells were also detected (Fig. 4B–E, arrows) but only very few in number. This replacement by GFP$^+$ fibers could be observed only from day 10 to day 20 and had dramatically decreased on day 30 (Fig. 2A, g–i). FISH analysis revealed a small number of GFP-DNAs in myonuclei (data not shown). These results indicated that the irradiation for myeloablation evoked muscle injury and that KSL cells engrafted in damaged muscles, fusing the host's muscle fibers, and participated in muscle regeneration in the early phase of transplantation.

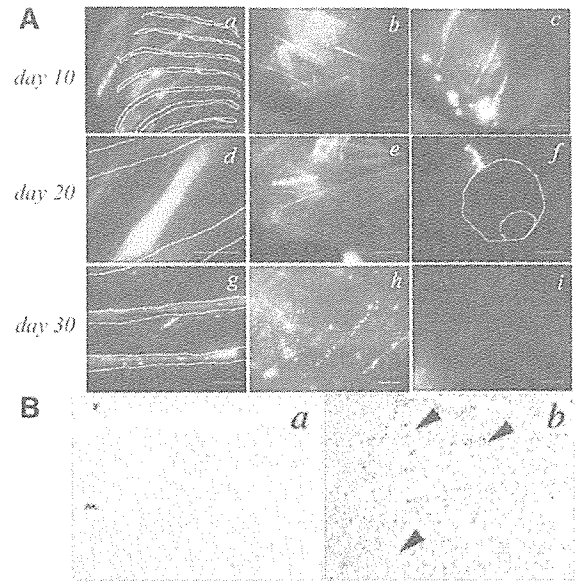

Figure 2. (A): Visualization of transplanted GFP$^+$ cells in muscles on days 10, 20, and 30. Appearances of various muscles under a fluorescent stereomicroscope are shown. Muscle tissues were removed from recipient mice and observed under a fluorescent stereomicroscope on days 10, 20, and 30 after transplantation. a, d, g: Intercostal muscle (the white lines indicate the shape of ribs). b: Abdominal muscle. c: Thigh muscle. e: Greater pectoral muscle. f: External ocular muscle (the white line indicates the shape of the eyeball). h: Dorsal muscle. Bars: a–c, e, 2 mm; d, 500 μm; f–g, i, 1 mm; h, 200 μm. **(B):** Immunohistostaining of the section of muscle tissues on day 10. a: Negative control. b: The section was stained with anti-GFP antibodies (alkaline phosphatase, faintly red region; arrowheads), and hematoxylin was used for nuclear staining.

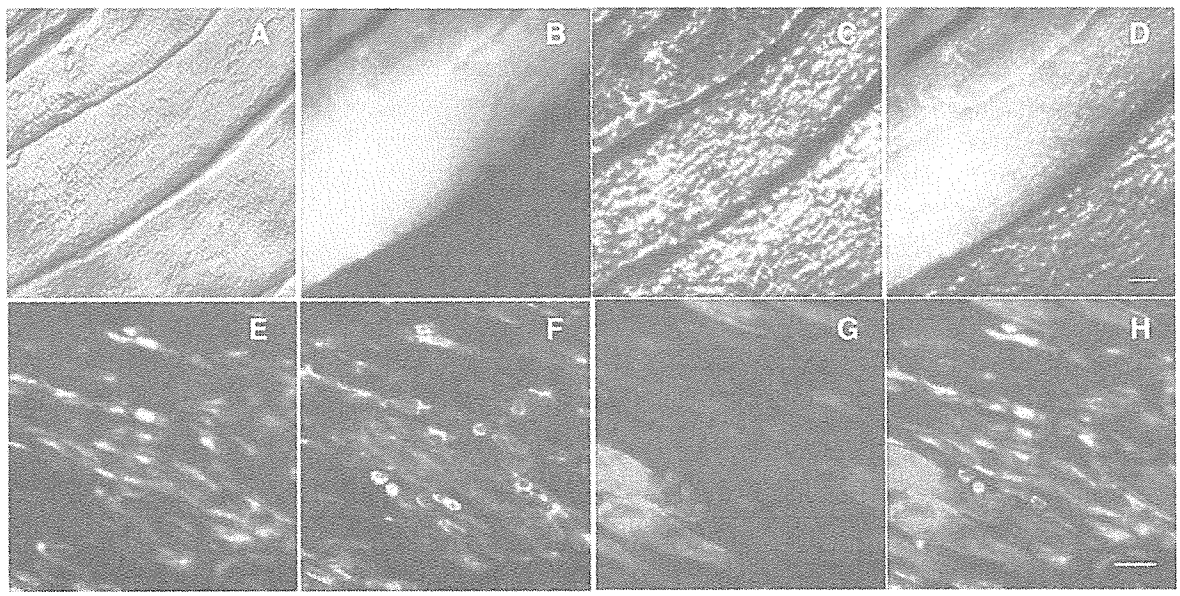

Figure 3. GFP$^+$ regions in intercostal muscle on day 20. Intercostal muscles were removed from recipient mice and fixed with 4% paraformaldehyde and made into frozen sections, as described in Materials and Methods. There were two types of GFP regions: **(A–D)** GFP$^+$ fibers and **(E–H)** GFP$^+$ mononuclear cells. Each section was stained with anti-GFP antibody (**B, D, E, H**, green), anti-myosin antibody (**C, D**, Cy3 red; **G, H**, Alexa350 blue), and anti-CD45 antibody (**F, H**, Cy3 red). **(A):** Phase contrast (**D, H**): Merge. Bars: D, 10 μm; H, 20 μm.

KSL Cells Settle in Muscle Tissue Like a Satellite Cell

Sections of the muscle tissues obtained 30 days and 6 months after transplantation were stained with anti-GFP and anti-laminin (a marker of the basal lamina) antibodies, showing that several GFP$^+$ cells were located inside the basal lamina with laminin expression (Fig. 5A), which is where satellite cells are usually found. GFP$^+$ cells under the basal lamina were coexpressed with c-Met antigen (a marker of satellite cells) (Fig. 5E, arrows). Furthermore, we isolated single fibers from soleus muscles 2 months after transplantation and stained them with anti-PAX7, MyoD, or Myf5, which are specific satellite cell markers. We detected Myf5$^+$GFP$^+$ satellite cells on the fibers (Fig. 6A–D), but neither PAX7$^+$GFP$^+$ cells nor MyoD$^+$GFP$^+$ cells (data not shown). These results suggested that GFP$^+$ KSL cells migrate into muscle tissues, with some of them localizing beneath the basal lamina expressing satellite cell markers.

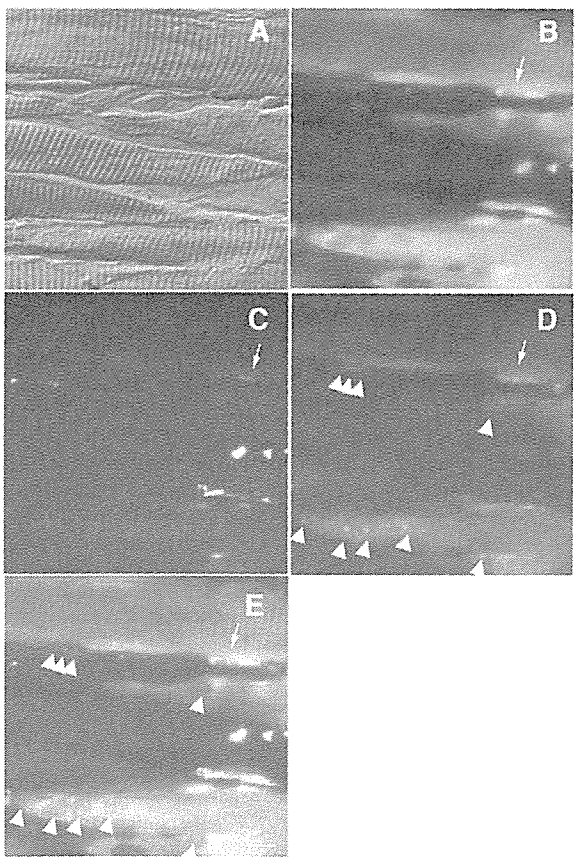

Figure 4. Myogenic phenotype of a CD45$^+$ cell in muscle tissues on day 20. **(A, B):** GFP$^+$ muscle structure showed cross striations. These sections were stained with anti-CD45 antibody (**C**, Cy3 red) and anti-myogenin antibody (**D**, blue). **(E):** Merge. Myogenin$^+$ myoblast- or myotube-like cells were detected (**D, E**, arrowhead), and an elongated GFP$^+$ cell coexpressed myogenin and CD45 (**B–E**, arrow).

KSL Cells Can Settle in Muscle Tissues Without Muscle Damage

Tissue-specific stem cells occupy niches—microenvironments that maintain self-renewal activity and multipotency of stem cells. Since it is known that irradiation depletes endogenous satellite cells and that injected muscle precursors can replace them [26], we used lethal irradiation for the transplantation assay. However, lethal irradiation also evokes various responses in the body. To exclude the influence of irradiation damage, we next transplanted KSL cells into W/W^v neonates. W/W^v mice possess a c-Kit gene mutation and can accept transplanted HSCs in a BM niche without irradiation [27]. Moreover, transplantation into W/W^v neonates results in a higher chimeric ratio than does transplantation into adults [28]. Our experiments using transplantation into W/W^v neonates showed no evidence of GFP$^+$ muscle fibers at any time, whereas BM cells were almost entirely replaced. However, small GFP$^+$ mononuclear cells could be detected between muscle fibers as early as 30 days after transplantation (Fig. 7A). Some GFP$^+$ cells were also detected beneath the laminin-positive basement

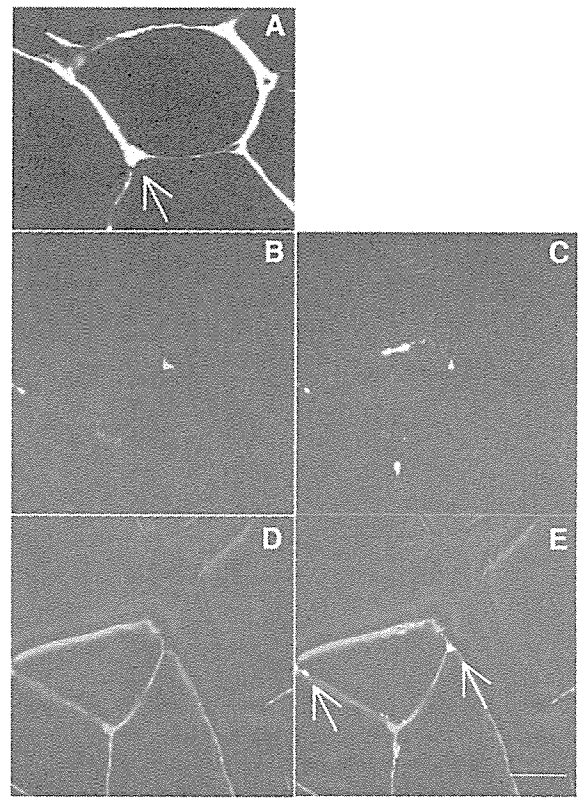

Figure 5. GFP$^+$ cells localized like satellite cells long term after transplantation. Sections from 6 months after transplantation were stained with laminin (**A**, Cy3 red; **D, E**, Alexa350 blue) and c-Met (**C, E**, Cy3 red) GFP$^+$ cells localized under the basal lamina (**A, E**, arrows) and were costained with c-Met (**E**, arrows). Bar: 20 μm.

membrane (Fig. 7B), and some of them were also stained with anti-c-Met antibody (Fig. 7C). We also examined isolated single fibers 1 month after transplantation and detected MyoD$^+$GFP$^+$ cells and PAX7$^+$GFP$^+$ cells on the fibers (Fig. 6H, L). We could also detect Myf5$^+$GFP$^+$ cells on the fibers 2 months after transplantation (Fig. 6P). These results showed that KSL cells and/or their progenies could migrate into undamaged muscle tissues expressing satellite cell–specific markers also, and that a suitable microenvironment for them might exist in skeletal muscles.

KSL-Derived Cells in Muscle Can Generate Muscle Fibers In Vitro in Long Term After Transplantation

So far it has been reported that damaged muscles by chemical agent or stress were regenerated by donor cells after BM transplantation [12, 15]. However, these muscle-regeneration assays in vivo cannot clarify whether donor cells participate in regenerating muscles directly from the settled muscle or indirectly from settled BM. To determine whether GFP$^+$ mononuclear cells in muscle tissues can differentiate into muscle fibers, a single-fiber culture was performed. Six months after transplantation with KSL cells,

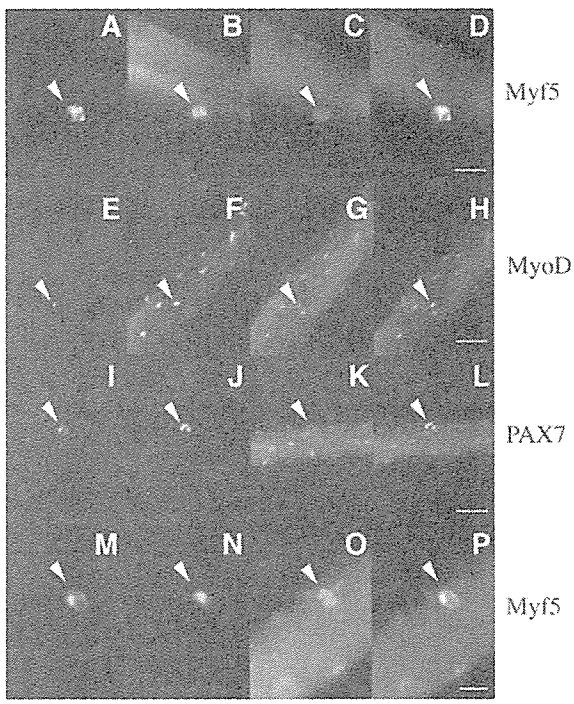

Figure 6. Immunostaining of single fibers. Single fibers were isolated from **(A–D)** irradiated mice 2 months after transplantation and from **(E–P)** W/W^v mice 1 or 2 months after transplantation and were stained with satellite cell–specific markers. **(A, E, I, M):** Anti-GFP antibody (FITC green, arrowheads). **(B, N):** Anti-Myf5 antibody (Cy3 red, arrowheads). **(F):** Anti-MyoD1 antibody (Cy3 red, arrowhead). **(J):** Anti-PAX7 antibody (Cy3 red, arrowhead). **(D, H, L, P):** Merge. Bars: D, P, 50 μm; H, L, 100 μm.

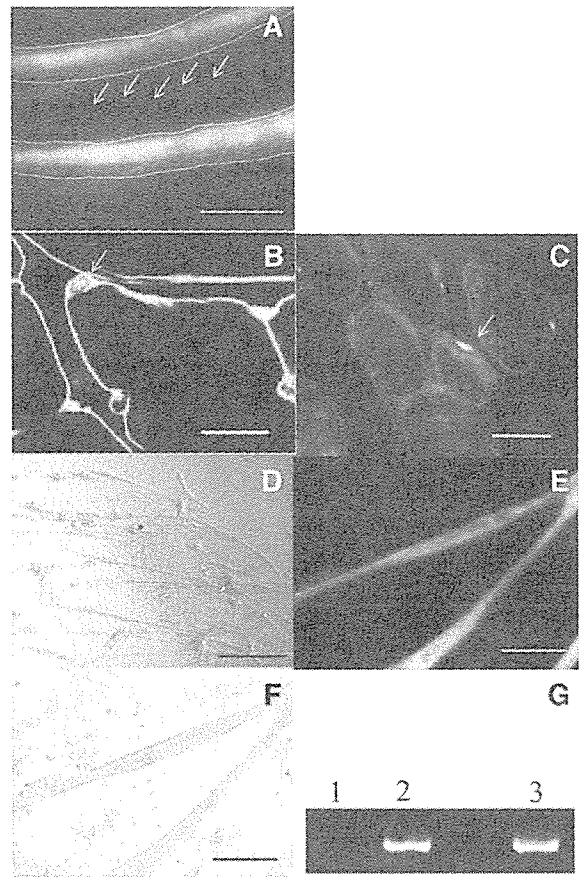

Figure 7. Analysis of the potential of GFP$^+$ satellite-like cells in muscle 6 months after transplantation. Thirty days and 6 months after nonirradiated transplantation into W/W^v neonates, GFP$^+$ mononuclear cells were detected between muscle fibers under fluorescent stereomicroscope (**A**, arrows). In the sections, immunostaining for laminin and c-Met was performed (**B, C**). **(A):** Appearance of rib and rib muscle under fluorescent stereomicroscope on day 30. Some GFP$^+$ mononuclear cells were detected (arrows). The white lines indicate the shape of ribs. **(B):** Immunohistochemistry with anti-laminin (Cy3 red) and anti-GFP antibodies. A confocal microscope was used to determine the precise location of GFP$^+$ cells. GFP$^+$ cells beneath basal lamina (arrow) were detected on day 30 and 6 months later. **(C):** GFP$^+$ cell under laminin-positive basal lamina (Alexa350 blue) was also stained with anti c-Met antibody (Cy3 red, arrow). **(D–F):** Single-fiber culture was performed with single fibers isolated from recipient mice 6 months after transplantation, followed by immunostaining. C, negative control; D, anti-myosin (Cy3 red) staining; E, anti-GFP-ALP (red) staining. D and E were same position. GFP-ALP$^+$ fibers were confirmed to be muscle fibers using myosin Cy3 staining. **(G):** PCR analysis of extracted DNA from single-fiber culture. DNA was extracted from the single-fiber culture followed by PCR for GFP DNA, as described under Materials and Methods. 1: negative control; 2: peripheral blood of GFP transgenic mouse; 3: single fiber culture. Bars: A, 1 mm; B, C, 20 μm; D, 200 μm; E, F, 50 μm.